Local anesthetics elicit immune-dependent anticancer effects

Lucillia Bezu, Alejandra Wu Chuang, Allan Sauvat, Juliette Humeau, Wei Xie, Giulia Cerrato, Peng Liu, Liwei Zhao, Shuai Zhang, Julie Le Naour, et al.

Journal for ImmunoTherapy of Cancer

Local anesthetics elicit immune-dependent anticancer effects

Lucillia Bezu ,[1,2,3] Alejandra Wu Chuang,[1,2] Allan Sauvat,[1,2] Juliette Humeau,[1,2,4,5] Wei Xie ,[1,2] Giulia Cerrato,[1,2] Peng Liu,[1,2] Liwei Zhao,[1,2] Shuai Zhang,[1,2] Julie Le Naour,[1,2] Jonathan Pol ,[1,2] Peter van Endert,[6] Oliver Kepp ,[1,2] Fabrice Barlesi,[7,8] Guido Kroemer[1,2,9]

To cite: Bezu L, Wu Chuang A, Sauvat A, *et al*. Local anesthetics elicit immune-dependent anticancer effects. *Journal for ImmunoTherapy of Cancer* 2022;**10**:e004151. doi:10.1136/jitc-2021-004151

► Additional supplemental material is published online only. To view, please visit the journal online (http://dx.doi.org/10.1136/jitc-2021-004151).

Accepted 22 March 2022

For numbered affiliations see end of article.

Correspondence to
Dr Lucillia Bezu;
lucilliabe@gmail.com

Guido Kroemer;
kroemer@orange.fr

ABSTRACT

Background Retrospective clinical trials reported a reduced local relapse rate, as well as improved overall survival after injection of local anesthetics during cancer surgery. Here, we investigated the anticancer effects of six local anesthetics used in clinical practice.

Results *In vitro*, local anesthetics induced signs of cancer cell stress including inhibition of oxidative phosphorylation, and induction of autophagy as well as endoplasmic reticulum (ER) stress characterized by the splicing of X-box binding protein 1 (XBP1s) mRNA, cleavage of activating transcription factor 6 (ATF6), phosphorylation of eIF2α and subsequent upregulation of activating transcription factor 4 (ATF4). Both eIF2α phosphorylation and autophagy required the ER stress-relevant eukaryotic translation initiation factor 2 alpha kinase 3 (EIF2AK3, best known as PERK). Local anesthetics also activated two hallmarks of immunogenic cell death, namely, the release of ATP and high-mobility group box 1 protein (HMGB1), yet failed to cause the translocation of calreticulin (CALR) from the ER to the plasma membrane. *In vivo*, locally injected anesthetics decreased tumor growth and improved survival in several models of tumors established in immunocompetent mice. Systemic immunotherapy with PD-1 blockade or intratumoral injection of recombinant CALR protein, increased the antitumor effects of local anesthetics. Local anesthetics failed to induce antitumor effects in immunodeficient mice or against cancers unable to activate ER stress or autophagy due to the knockout of EIF2AK3/PERK or ATG5, respectively. Uncoupling agents that inhibit oxidative phosphorylation and induce autophagy and ER stress mimicked the immune-dependent antitumor effects of local anesthetics.

Conclusion Altogether, these results indicate that local anesthetics induce a therapeutically relevant pattern of immunogenic stress responses in cancer cells.

Key messages

What is already known on this topic

► Retrospective trials observed an improved survival after the use of local anesthetics during oncological surgery. The mechanisms by which these agents may exert an antitumor activity remain unclear.

What this study adds

► Local anesthetics elicit direct and immune antitumor effects potentiated by immunotherapy.

How this study might affect research, practice or policy

► The immune property of local anesthetics could be used during surgical procedures to control migrating residual cancer cells and opens up a novel field of research called onco-anesthesia.

INTRODUCTION

Cancer results from two interlinked and age-dependent processes: (1) the genetic and epigenetic instability of cells activating oncogenes and inactivating tumor suppressor genes and (2) the loss of immunosurveillance mechanisms that usually eliminate or control neoplastic cells.[1 2] As a result, modern anticancer agents have been designed to suppress oncogenic pathways or to (re)activate anticancer immune responses.[3 4] Moreover, chemotherapeutic agents have turned out to be particularly efficient when they succeed in not only reducing tumor mass but also inducing antitumor immunity.[5–7] Often such immunostimulatory effects are obtained secondary to chemotherapy-mediated activation of stress pathways such as autophagy and elements of the endoplasmic reticulum (ER) stress response before cell death occurs.[8–11] Such stress-related and lethal pathways cause the emission of immunostimulatory danger-associated molecular patterns (DAMPs), in particular adenosine triphosphate (ATP, the release of which is favored by autophagy),[12 13] calreticulin (CALR, the exposure of which is favored by partial induction of ER stress)[8 14] and HMGB1 (the release of which is associated with cell death).[15] Cancer cells in which these stress responses and DAMPs release or exposure pathways are interrupted become resistant to chemotherapy because of their failure to activate a specific immune response.[5 8] In sum, it appears that therapy-elicited immunosurveillance plays a major role in determining the outcome of the clinical management of oncological disease.

Hitherto unsuspected external factors affect the immune-cancer dialogue. For example, induction of stress hormones including catecholamines and glucocorticoids,[16] perturbation of the gut microbiota by broad-spectrum antibiotics[17–19] and other co-medications including beta-blockers modulate the clinical efficacy of anticancer treatments.[20–22] In this context, it would not be surprising that surgical interventions with their components of mental, nutritional, mechanic and inflammatory distress as well as the associated polypharmacy (including the administration of antibiotics, benzodiazepines, non-steroidal anti-inflammatory drugs, general and local anesthetics, vasoactive amines, glucocorticoids…) would affect anticancer immunosurveillance, as suggested by statistically significant epidemiological associations.[23–34]

Here, we investigated the possible impact of several local anesthetics that are currently used in the clinics on cancer immunosurveillance in preclinical models. For this, we determined the effects of six local anesthetics on immunogenic cancer cell stress pathways and determined their possible antineoplastic effects by injecting them into established tumors. We found that local anesthetics induce autophagy and facets of ER stress that are immunostimulatory, hence favoring an immune-dependent reduction of tumor progression.

MATERIALS AND METHODS

Cell lines

Human osteosarcoma U2OS, human cervical cancer HeLa, murine colon adenocarcinoma MC38 and murine breast cancer E0771 cells were purchased from the ATCC. Murine fibrosarcoma MCA205 cells were purchased from Merck. U2OS cells stably expressing HMGB1-GFP; MITOdsRED; GFP-LC3; GFP-LC3 *Atg5*$^{-/-}$; RFP-LC3; mCherry-GFP-LC3; pSMALB-ATF4.5rep, XBP1ΔDBD-venus-RFP-FYVE; GFP-LC3 EIF2AK1$^{-/-}$; EIF2AK2$^{-/-}$; EIF2AK3$^{-/-}$; EIF2AK4$^{-/-}$; RFP-LC3 eIF2α^{S51A} (mutant with non-phosphorylable version of eIF2α) and murine fibrosarcoma MCA205 EIF2AK3$^{-/-}$; MCA205 Atg5^{KD}, MCA205 CD39 were generated by our group in the past (Michaud *et al*, 2011; Shen *et al*, 2012; Zhou *et al*, 2016; Bezu *et al*, 2018; Humeau *et al*, 2020). U2OS GFP-ATF6 cells were a kind gift from Prof. Peter Walter (University of California, San Francisco, USA). Cell lines were frequently tested for mycoplasma contamination.

Cell culture

U2OS cell lines were cultured in Dulbecco's modified Eagle's medium (#41 966-02, Thermo Fisher Scientific) supplemented with 10% fetal bovine serum (#F7524, Sigma Aldrich), 1% non-essential amino acids (#11 140-035, Thermo Fisher Scientific), 1% HEPES (#15630080, Thermo Fisher Scientific) and 1% penicillin/streptomycin (#15140122, Thermo Fisher Scientific). For U2OS HMGB1-GFP, XBP1ΔDBD-venus-RFP-FYVE, GFP-LC3 and GFP-ATF6 0.5 mg/mL G418 (#10 131-27, Thermo Fisher Scientific) was added to the medium. MCA205 cell lines were cultured in Roswell Park Memorial Institute (RPMI) 1640 medium (#61870044, Thermo Fisher Scientific) supplemented with identical components. Cells were maintained in a humidified incubator at 37°C with 5% CO_2. Cell culture consumables were purchased from Corning (New York, USA).

Compounds

Antimycin A (A8674), BAY87-2243 (SML2384), bupivacaine (B5274), carbonyl cyanide m-chlorophenylhydrazone (C2759), carbonyl cyanide 4-(trifluoromethoxy) phenylhydrazone (C2920), chloroprocaine (1117008), dactinomycin (A1410), 2-deoxyglucose (D3179), 2,4-dinitrophenol (D198501), erastin (E7781), ferrostatin (SML0583), glucose (G7021), levobupivacaine (SML1092), lidocaine (L5647), mitoxantrone (M6545), necrostatin (N9037), oligomycin A (75351), prilocaine (P9547), ropivacaine (R0283), rotenone (557368), staurosporine (S6942), TNF-alpha (T6674), thapsigargin (T9033), tunicamycin (T7765) have been purchased from Merck-Sigma Aldrich. Oxaliplatin was purchased from Accord Healthcare (Ahmedabad, India). Bafilomycin A1 (1334), rapamycin (1292), torin 1 (4247) were purchased from Tocris bioscience (Bristol, UK). Smac-BV6 was purchased from CliniSciences (B4653), z-VAD-fmk (N1510.0025) was purchased from Bachem. Recombinant calreticulin was produced as described.[8 14]

Antibodies

Rabbit polyclonal antibody CALR (ab2907), rabbit monoclonal phosphoneoepitope-specific antibody against phospho-eIF2α (Ser 51) (ab32157, clone E90), mouse monoclonal antibody against β-actin (ab49900, clone AC-15) were purchased from Abcam (Cambridge, UK). Rabbit polyclonal antibody against HRI (sc-30143), mouse monoclonal antibody against PKR (sc-6282, clone B-10) were purchased from Santa-Cruz biotechnology. Rabbit monoclonal antibody against PERK (#3192, clone C33E10), rabbit polyclonal antibody against GCN2 (#3302), rabbit polyclonal antibody against eIF2α (#99 722 S), rabbit monoclonal antibody against LC3B (#2775), rabbit polyclonal antibody against GFP (#2555) were purchased from Cell Signaling Technology (Danvers, MA, USA). Antibody anti-PD-1 (BE0273, clone 29F.1A12) and rat IgG1 anti-horseradish peroxidase isotype control (BE0088, clone HRPN) were purchased from BioXcell (West Lebanon, NH, USA). Mouse monoclonal antibody against Atg5 (A2859) was purchased from Merck-Sigma Aldrich. Anti-rabbit Alexa fluor®−488 coupled secondary antibody came from Thermo Fisher Scientific (#A11034). APC anti-mouse CD11c (Clone N418) was purchased from Biolegend (117310).

Determination of IC_{20} and IC_{50}

U2OS cells were seeded at 1,500 cells per well in 384-well plates (Greiner Bio-one; Kremsmünster, Austria). The day after, cells were treated at different concentrations for 8 hours. Then, cells were washed once with PBS and fixed

in 3.7% formaldehyde (F8775, Merck Sigma Aldrich) supplemented with 1 µg/mL Hoechst 33 342 (H3570, Thermo Fisher Scientific) for 20 min. After washing with PBS, plates were immediately analyzed by fluorescence microscopy. Micrographs were analyzed with R by means of the *EBImage package*. Notably, nuclei were detected using the Hoechst staining from which average nuclear size and intensity were computed. These parameters were subsequently used to cluster cells as healthy cells (normal-sized nucleus, Hoechst^{dim}) and dead cells (condensed nucleus, Hoechst^{bright}). The number of dead cells was used to determine a dose-response curve by fitting the data point with a 4-parameter log-logistic function. This curve was used to determine the IC_{20} (concentration at which 20% of cells are dead) and the IC_{50} (concentration at which 50% of cells are dead) for each drug.

Western blot

Extraction of proteins was realized in RIPA buffer (#89900; Thermo Fisher Scientific) associated with phosphatase and protease inhibitors (#88669; Thermo Fisher Scientific). Protein content was measured by Bio-rad laboratory DCTM Protein Assay reagent A, B and S (#500-0113, #500-0114 and #500-0115). A minimum of 15 µg of protein was solved in Laemmli buffer (Thermo Fisher Scientific), denaturated at 100°C and separated by electrophoresis using 4%–12% Bis-Tris gels (Thermo Fisher Scientific) in MES buffer (Thermo Fisher Scientific). Then, proteins were transferred to nitrocellulose membrane (Merck Millipore IPVH00010) in transfer buffer (25 mM Tris; 190 mM glycine; 20% methanol in H_2O) at 200 mA for 1.5 hour. Membranes were washed in Tris-buffered saline with Tween20 buffer (TBST; 20 mM Tris, pH 7.5 150 mM NaCl 0.1% Tween 20 in H_2O) and treated with blocking buffer (5% bovine serum albumin (BSA) in TBST) for 1 hour. Membranes were exposed to primary antibody diluted in 5% BSA in TBST overnight at 4°C. The day after membranes were washed with TBST and incubated with appropriate horseradish peroxidase-coupled secondary antibody (Southern Biotech, Birmingham, Alabama, USA) for 1 hour at room temperature. Then proteins were revealed with ECL (GE Healthcare, Chicago, Illinois, USA). β-actin (1:10,000) was used to verify equal protein loading.

Fluorescence microscopy, image acquisition and analysis

One day before treatment, 1,500 U2OS cells either wild-type or stably expressing ATF6-GFP, GFP-LC3; GFP-LC3 *Atg5*$^{-/-}$; RFP-LC3, mCherry-GFP-LC3, pSMALB-ATF4.5rep, XBP1ΔDBD-venus-RFP-FYVE, GFP-LC3 EIF2AK1$^{-/-}$, EIF2AK2$^{-/-}$, EIF2AK3$^{-/-}$, EIF2AK4$^{-/-}$ or RFP-LC3 eIF2α^{S51A} were seeded in 384-well plates (Greiner Bio-one; Kremsmünster, Austria). Upon treatment cells were washed once with PBS and fixed in 3.7% formaldehyde (F8775, Merck Sigma Aldrich) supplemented with 1 µg/mL Hoechst 33 342 (H3570, Thermo Fisher Scientific) for 20 min. ATF6-, XBP1-, pSMALB-ATF4.5rep-, LC3-, FYVE-expressing cells were immediately analyzed by fluorescence microscopy. For the analysis of eIF2α phosphorylation, cells were washed once with PBS after fixation and primary antibody diluted in blocking buffer (1:250, 2% BSA in PBS) was added for overnight at 4°C.[35] Following, cells were washed thrice with PBS and incubated with AlexaFluor®-coupled secondary antibody (Thermo Fisher scientific) diluted 1:1,000 in 2% BSA for 45 min. Then, cells were washed once with PBS and fluorescence microscopic analyses were performed. A 20X PlanAPO objective (Nikon, Tokyo, Japan) was used for acquisition of four view fields per well. An automated image processing with the Custom Module Editor from MetaXpress Software (Molecular Devices) was used for image segmentation. Primary nuclear region of interest (ROI) was designed by a mask around the nucleus for cell count and for Hoechst, ATF4 or ATF6 fluorescence quantification. A secondary cytoplasmic ROI was used for the fluorescence intensity of phospho-eIF2α, ATF6, XBP1s or LC3 dots count. After exclusion of debris and dead cells, data were normalized and statistical analyses were performed with R software. Scale bars represent 10 µm.

SiRNA interference

Seven hundred and fifty U2OS wild-type cells were seeded in a 96-well plate. The next day, cells were transfected with small-interfering RNAs targeting *Atg5* gene (ON-TARGETplus SMART pool SiRNA ATG5, L-004374-00-0005, Dharmacon, Lafayette, CO, USA) for 24 hours at a final concentration of 10 µM by means of DharmaFECT^{TM} transfection reagent according to the manufacturer's instruction (SMARTpool of 4 individual siRNAs). At day 3, medium was discarded. Cells were used at day 5.

Extracellular ATP quantification

Eight thousand U2OS wild-type cells per well were seeded in a 96-well plate. The next day, cells were treated for 24 hours. Then the supernatant was collected, centrifuged and transferred to a white bottom 96-well plate. Enzyme and substrate from ENLITEN ATP Bioluminescence Detection Kit (FF2000; Promega, Madison, Michigan, USA) were added. ATP-dependent substrate conversion was measured by luminescence at 560 nm with a Spectramax I3 multimode plate reader (Molecular Devices).

Calreticulin exposure by flow cytometry

Eight thousand U2OS wild-type cells per well were seeded in a 96-well plate. After 6 hours of treatment, cells were collected and transferred into a V-shape 96-well plate and centrifuged at 12,000 rpm for 5 min. Supernatant was removed and cells were incubated for 30 min at 4°C with primary rabbit monoclonal antibody against CALR (1:100 diluted in 1% BSA). Cells were washed, centrifuged at 12,000 rpm for 5 min and supernatant was removed. Cells were incubated with secondary AlexaFluor®488 goat anti-rabbit IgGs (1:1,000 diluted in BSA 1%) for 30 min at 4°C. Cells were washed, centrifuged at 12,000 rpm for 5 min and supernatant was removed. Finally, diamidino-2-phenylindole (DAPI,

#62248, Thermo Fisher Scientific) was added before the analysis (1:400). Samples were analyzed using a CyAn ADP cytofluorometer (Beckman Coulter, Brea, California, USA) coupled to a HyperCyt loader (Intellicyt, Albuquerque, New Mexico, USA).

HMGB1 release by videomicroscopy

One day before treatment, 2×10^3 U2OS stably expressing HMGB1-GFP and H2B-RFP per well were seeded in a 384-well plate. The next day, cells were treated and observed by live-cell microscopy with a frequency of 1 image by hour for 24 hours. Then images were segmented and analyzed with R using the *EBImage package*. H2B-RFP was used to segment nuclei. Then, the obtained mask was used to measure nuclear GFP intensity over time, thus allowing to calculate the average signal loss.

Cell death assessment by flow cytometry

Eight thousand U2OS cells per well were seeded in a 96-well plate. After 8 hours of treatment, supernatant and cells were collected and transferred into a V-shape 96-well plate and centrifuged at 12,000 rpm for 5 min. Then, cells were incubated with diamidino-2-phenylindole (DAPI 0.5 µg/mL, #62248, Thermo Fisher Scientific) and with 3,3'-dihexyloxacarbocyanine iodide (DIOC 20 nM, #D273, Thermo Fisher Scientific) for 20 min at 37°C. Samples were analyzed using a CyAn ADP cytofluorometer (Beckman Coulter, Brea, California, USA) coupled to a HyperCyt loader (Intellicyt, Albuquerque, New Mexico, USA).

Autophagic flux measurement by U2OS mCherry-GFP-LC3 tandem reporter

To assess autophagic flux, U2OS cells stably expressing a tandem reporter mCherry-GFP-LC3 were seeded in a 96-well plate. The next day, cells were treated for 24 hours and observed by live-cell microscopy with a frequency of 1 image by hour for 24 hours. Then images were segmented and analyzed with R using *EBImage package*. The mCherry-GFP-LC3 tandem reporter emits GFP and mCherry signals in autophagosomes yet changes its fluorescence properties in the acidic environment upon lysosomal fusion. In consequence, the tandem reporter emits and solely mCherry signal in autolysosomes thus indicating autophagic flux.

Mitochondrial fiber assessment by videomicroscopy

One day before treatment, 8×10^3 U2OS stably expressing MITOdsRED were seeded in each well of a 96-well plate. Cells were stained with 3,3′-dihexyloxacarbocyanine iodide (DIOC 20 nM, #D273, Thermo Fisher Scientific) for 30 min. Then, cells were washed, treated and observed by live-cell microscopy with a frequency of 2 images by hour for 36 hours. Finally, images were segmented and analyzed with R using *EBImage package*. Briefly, the mitochondrial mask was detected using dsRed signal, and then skeletonized to measure the total length of the network.

Oxygen consumption

Oxygen consumption rate (OCR) measurements were performed using the Seahorse XFe96 Flux Analyzer and the XF cell Mito stress kit (SeaHorse Agilent, Santa Clara, California, USA) as previously described by our group (Sica *et al*, 2017). Briefly, 8×10^3 U2OS wild-type cells per well were seeded in a 96-well plate and treated for 6 hours. Then, cells were incubated with 200 µL/well of SeahorseXF assay medium (102365-100) (pH 7.4) containing 2 mM glutaMAX, supplemented with 10 mM glucose and 1 mM sodium pyruvate for 1 hour at 37°C without CO_2. Then the cartridge was loaded with oligomycin A (27 mM), carbonyl cyanidem-chlorophenyl hydrazine (CCCP, 3 mM) and rotenone (13.75 mM) which the Seahorse apparatus injected sequentially while measuring the OCR.

Glycolytic flux

Extracellular acidification rate (ECAR) measurements were performed using the Seahorse XFe96 Flux Analyzer and the XF cell Glycolysis kit (SeaHorse Agilent) as previously described by our group (Sica *et al*, 2017). Briefly, 8×10^3 U2OS wild-type cells per well were seeded in a 96-well plate and treated for 6 hours. Then cells were incubated with 200 µL/well of Seahorse XF assay medium (102365-100) (pH 7.4) for 1 hour at 37°C without CO_2. Then the sensor cartridge was loaded with glucose (90 mM), oligomycin A (30 mM) and 2DG (200 mM) which the Seahorse apparatus injected sequentially while measuring the ECAR.

Measurement of transcription inhibition

Evaluation of transcription was assessed using two distinct methods: the incorporation of Click-iT chemistry-detectable 5-ethynyl uridine (EU) (#C10327, Thermo Fisher Scientific) measured as described in (Cerrato *et al*, *in press*[36]), as well as transmitted-light based cell image classification using trained deep neural networks, as described in Sauvat *et al*.[37] Two thousand human osteosarcoma U2OS cells per well were seeded in 384-well µClear imaging plates (Greiner Bio-One) and let adhere for 24 hours. The following day, cells were pre-treated for 2.5 hours and then the treatment pursued in the presence of 1 mM EU for an additional hour. Cells were then fixed with 3.7% formaldehyde containing 1 µg/mL Hoechst 33 342 for 1 hour at room temperature and permeabilized with 0.1% Triton X-100 for 10 min. Alexa-Fluor®488-coupled azide was then added for 2 hours at room temperature following the manufacturer's instructions. The EU intensity corresponding to the GFP signal in the nucleus was measured by fluorescence microscopy. Nuclear GFP values of each condition were normalized to the untreated control, and the percentage of transcription inhibition was calculated. In parallel, transmitted light images were acquired and a dual deep-learning algorithm was applied to classify cells based on their nuclear phenotype. Briefly, cell nuclei were first segmented using a pre-trained Fully Convolutional Neural Network (FCNN), allowing the

extraction of single-cell patches, and thereafter classified using a Deep Convolutional Neural Network (DCNN) in a binary fashion as 'inhibited' or 'control' phenotypes. The percentage of nuclei bearing a transcription inhibition phenotype was calculated.

Assessment of phagocytosis

Phagocytosis was assessed as previously described.[38] Bone marrow-derived dendritic cells (BMDCs) were provided from femurs of C57Bl/6 mice. Bone marrow was collected by flushing the bones with PBS, and clusters were dissolved by pipetting. Then, red blood cells were lysed with red cell lysis buffer (0.01 M Tris, 0.83% NH_4Cl in Milli-Qwater). After washing and filtration, 1.5×10^6 viable cells were seeded into 6-well plates in 2 mL of BMDC culture medium (RPMI 1640 medium supplemented with 10% fetal bovine serum, 1% non-essential amino acids, 1% HEPES and 1% penicillin/streptomycin and 50 µM β-mercaptoethanol) supplemented with 20 ng/mL recombinant mouse GMCSF and 5 ng/mL IL-4. At day 6, half of the supernatant was removed and replaced by the original culture. Non-adherent BMDCs were harvested on day 7, counted, and 8×10^5 mouse fibrosarcoma MCA205 cells were cultured in standard 25 cm^2 flasks for cell culture. The day after, MCA205 cells were labeled with 0.5 µM CellTracker Orange CMTMR (5-(and-6)-(((4 chloromethyl)benzoyl) amino) tetramethylrhodamine) dye (#C2927, Thermo Fisher Scientific) for 30 min at 37°C. Then, MCA205 cells were treated for 24 hours. After treatment, MCA205 cells were co-cultured with BMDCs in 6-well plates at 37°C at a 1:4 ratio (BMDC: MCA205) for 4 hours. Finally, cells were detached and BMDCs were stained with conjugated 1:100 anti-CD11c antibody diluted in 1% BSA for 30 min at 4°C in the dark. Cells were washed three times and fixed in 3.7% formaldehyde. Samples were analyzed through a BD LSRFortessa flow cytometer and acquired with a BD FACS-Diva software (BD Biosciences). Phagocytosis was determined by assessing the ratio of $CMTMR^+$ $CD11c^+$ cells over total amount of $CD11c^+$ BMDCs (FlowJo software and R software).

In vivo experiments

Female wild-type C57Bl/6 and *nu/nu* mice aged 6–8 weeks old were purchased from Envigo (Huntington, UK) and were kept in a pathogen-free animal facility with temperature-controlled environment. Mice received water and food ad libitum. The number of mice needed in each group was determined by 'BiostatTGV' software. Mice were randomized in each group based on tumor size before treatment. Tumor area was calculated with the formula length × width x π/4. Mice were sacrificed at a tumor size between 200 and 250 mm^2 or upon appearance of any signs of discomfort. Tumor growth and survival were analyzed with TumGrowth software package[39] available at https://github.com/kroemerlab.

In vivo tumor treatment

Murine MCA205 fibrosarcoma tumors were generated by subcutaneous (*s.c.*) injection of 1×10^5 cells into C57Bl/6 mice and *nu/nu* mice. Murine MCA205 *EIF2AK3*$^{-/-}$ fibrosarcoma tumors were generated by *s.c.* injection of 1×10^6 cells into C57Bl/6 mice. MCA205 *Atg5*^{KD} fibrosarcoma tumors were generated by *s.c.* injection of 1×10^6 cells into C57Bl/6 mice. Tumors from MCA205 cells expressing transgenic ectoATPase CD39 were generated by *s.c.* injection of 1×10^5 cells into C57Bl/6 mice. Murine E0771 breast tumors were generated by *s.c.* injection of 1×10^6 cells into C57Bl/6 mice. Murine MC38 colon tumors were generated by *s.c.* injection of 1×10^6 cells into C57Bl/6 mice. When tumors became palpable, mice were randomized in experimental groups and treated with 25 µL of local anesthetics or CCCP or FCCP (diluted in PBS) injected intratumorally (*i.t.*) once a day for 2 days. Tumor growth and weight were monitored frequently.

In order to boost the immune response, the same treatment was combined with immune checkpoint blockade. At days 8, 12 and 16 after the first injection of local anesthetics or CCCP or FCCP, 200 µg/mouse of anti-PD-1 or corresponding isotype (diluted in 100 µL PBS) were injected intraperitoneally.

Alternatively, mice with palpable MCA205 fibrosarcomas were treated by *i.t.* injection of ropivacaine (4 mg/kg) or CCCP (0.25 mg/kg) in a volume of 25 µL supplemented with recombinant calreticulin (15 µg/mouse) once a day for 2 days.

Profiling of the tumor-infiltrating T lymphocytes

MCA205 fibrosarcoma tumors were generated by subcutaneous (*s.c.*) injection of 1×10^5 cells in C57Bl/6 mice. When tumors became palpable, 25 µL of PBS or lidocaine (3 mg/kg) or ropivacaine (4 mg/kg) were injected intratumorally (*i.t*). At day 9, tumors were harvested, weighed, and then processed before phenotyping as described in[40]. In short, tumors were mechanically and enzymatically dissociated with the tumor dissociation kit (Miltenyi) and the gentle MACS Octo Dissociator (Miltenyi). Tumor cell homogenates were filtered and washed twice with ice-cold PBS. Then, homogenates corresponding to 50 mg of the initial tumor sample, were stained with LIVE/DEAD Fixable Yellow dead cell stain (Thermo Fisher Scientific) and Fc receptors were blocked with anti-mouse CD16/CD32 (clone 2.4G2, Mouse BD Fc Block, BD Pharmingen). T lymphocytes were phenotyped with a set of fluorochrome-conjugated antibodies as follow. First, surface receptors were stained with anti-CD45 APC-Fire750 (clone 30F-11, Biolegend), anti-CD3 APC (clone 17A2, BioLegend), anti-CD4 PerCP-Cy5.5 (clone RM4-5, Thermo Fisher Scientific), anti-CD8a PE (clone 53–6.7, BD Pharmingen), anti-CTLA4/CD152 APC (clone UC10-4F10-11, BD Pharmingen), anti-GITR/CD357 BV785 (clone DTA-1, BD Pharmingen), anti-ICOS/CD278 BV421 (clone 7E.17G9, BD Pharmingen), anti-LAG3/CD223 BV605 (clone C9B7W, BP Pharmingen), anti-PD-1/CD279 APC-Fire750 (clone 29F.1A12, Biolegend), anti-TIGIT BV711 (clone 1G9, BD Pharmingen), anti-TIM3/CD366 PeCy7 (clone RMR3-23, Invitrogen), anti-VISTA PercP-Cy5.5 (clone MH5A, Biolegend). Second, after

permeabilization of the cells in eBioscience FoxP3/Transcription Factor Staining Buffer (Thermo Fisher Scientific), intranuclear staining of the transcription factor FoxP3 was performed with anti-FoxP3 FITC (clone FJK-16s, Thermo Fisher Scientific). Stained samples were run through a BD LSRFortessa flow cytometer. All samples were acquired using BD FACSDiva software (BD biosciences) and analyzed using GraphPad Prism software.

Statistical analyses

In vitro, data of each experiment are presented as the mean of quadruplicates (or triplicates after automatic detection of outliers). Data are presented as mean±SD if one experiment representative of three independent experiments is shown. Data are presented as mean±SEM when resulting from three independent experiments. Statistical analyses were performed with R software (https://www.r-project.org). Student's *t*-test was used to compare parametric data to a control using the *t.test* function from the *stats* R package. A pairwise multiple comparison test (Benjamin-Hochberg correction) was applied to compare each condition to another in a dataset with the *pairwise.t.test* function from the *stats* R package. Heatmaps were generated after sigmoidal scaling of raw data. *In vivo*, statistical analyses were performed with the TumGrowth software package[39] available at https://github.com/kroemerlab. This R package allows for longitudinal analyses over entire segments of the tumor growth curves that can be subjected to automatic analyses of breakpoints in the tumor growth characteristics and outlier detection (if required). A type II analysis of variance (ANOVA) test and pairwise Wilcoxon test (with multiple comparison) were performed for tumor growth and a log-rank test was used for survival analysis. Tumor immune infiltrates were statistically evaluated with GraphPad Prism software. Samples were compared using a one-way ANOVA (Tukey's multiple comparisons test). Outliers were excluded based on the ROUT test (Q=10%). For all test, significance was assessed for $^{*/\#/\$}p<0.05$, $^{**/\#\#/\$\$}p<0.01$, $^{***/\#\#\#/\$\$\$}p<0.001$.

RESULTS

Induction of autophagy and cell death by local anesthetics *in vitro*

Human osteosarcoma U2OS cells are widely used in cell biology due to their large size, flat morphology, and strong adherence to microscopy-compatible plastic surfaces.[41] These cells have been equipped with multiple biosensors to explore immunology-relevant cell stress pathways including autophagy and the three arms of the ER stress response[9 42 43]. In a first step, we determined the dose at which six different local anesthetics would cause the death of 20% cells within 8 hours of culture (online supplemental figure S1A-F). The dose required for killing 20% of cells (IC_{20}) was in the range between 1.04 and 4.58 mM, depending on the anesthetic, for U2OS cells, in the same order of magnitude as for human cervical cancer HeLa cells (online supplemental figure S1G-L), for which a similar order of cytotoxic effects was determined (ranking the IC_{20} for both cell lines: levobupivacaine <bupivacaine < ropivacaine <chloroprocaine < prilocaine <lidocaine) (online supplemental figure S1A–L). We then determined the effects of each local anesthetic on cell stress at the IC_{20}, while focusing our analysis on the 80% of viable cells (by excluding dead cells with condensed nucleus, $Hoechst^{bright}$). U2OS cells that were either autophagy competent (wild type) or autophagy deficient (due to the knock-out of the *Atg5* gene) were equipped with autophagy biosensor microtubule-associated proteins 1A/1B light chain 3B (LC3) fused to green fluorescent protein (GFP) (figure 1A) and then cultured either in control condition or in the presence of the potent autophagy inducer rapamycin to observe the formation of GFP-positive autophagic *puncta* in the cytoplasm. Similar to the positive control, rapamycin, the six local anesthetics all induced the formation of discrete autophagic *puncta* in wild type, but not in $Atg5^{-/-}$ cells (figure 1B,C). The induction of GFP-LC3 *puncta* was observed at the IC_{20} as well as at slightly lower doses (online supplemental figure S2A, B). Moreover, the six anesthetics used at the IC_{20} caused the lipidation of endogenous LC3 protein that leads to an increase in the electrophoretic mobility of LC3 detectable by immunoblot (as LC3-II) and that is coupled to redistribution of LC3 from the cytosol to autophagosomes and autolysosomes.[44] Again, the generation of LC3-II was found to be *Atg5*-dependent (figure 1D and E). In addition, local anesthetics gave rise to the autophagy-associated phosphorylation of phosphatidylinositol (yielding phosphatidylinositol 3-phosphate, PI_3P) that is detectable by means of a biosensor composed by FYVE zinc finger domain fused to red fluorescent protein (RFP).[45] Indeed, the six local anesthetics caused the redistribution of RFP-FYVE toward cytoplasmic dots (online supplemental figure S2C, D). Moreover, the local anesthetics induced autophagic flux measured by means of a tandem mCherry-GFP-LC3 reporter that distinguishes autophagosomes (*puncta* with a red +green fluorescence) from autolysosomes (*puncta* with a purely red fluorescence due to quenching of GFP-dependent fluorescent signal at a low pH).[46] Indeed, bupivacaine, levobupivacaine, lidocaine and ropivacaine induced an increase in the ratio of autolysosomes over lysosomes that was reverted by simultaneous exposure to the lysosomal inhibitor bafilomycin A1, indicative of the induction of autophagic flux (online supplemental figure S2E, F). In summary, local anesthetics induce signs of autophagy in cancer cells.

Induction of ER stress by local anesthetics

Autophagy is tied to the induction of the integrated stress response, which is part of the ER stress response and consists in the phosphorylation of eukaryotic initiation factor 2α (eIF2α) on serine 51.[47–49] Local anesthetics (used at the IC_{20}, 8 hours) induced eIF2α phosphorylation detectable by means of a phospho-neoepitope specific

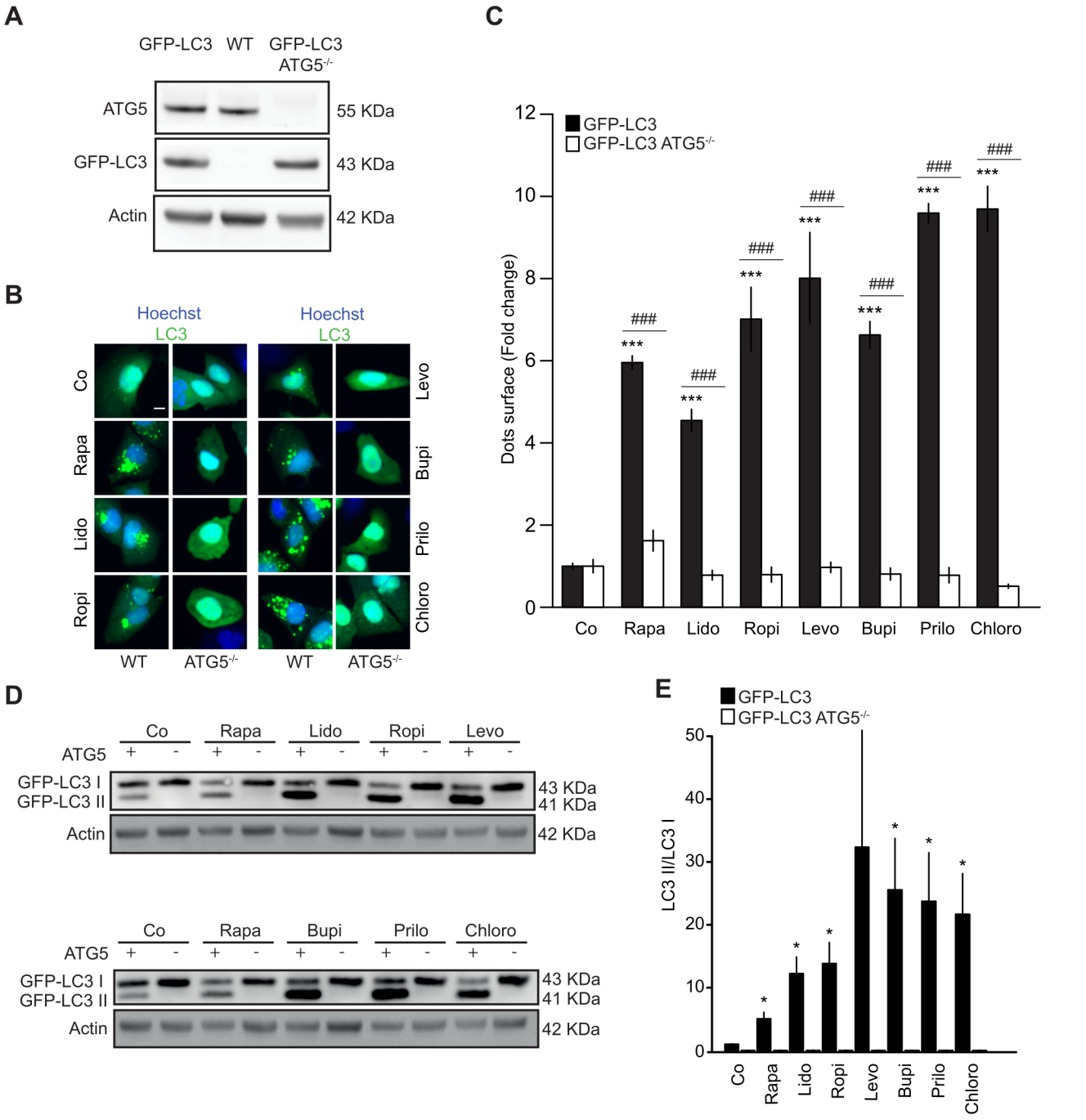

Figure 1 Local anesthetics induce autophagy in cancer cells A–E. human osteosarcoma U2OS wild-type cells, U2OS cells stably expressing GFP-LC3 and U2OS cells stably expressing GFP-LC3 knock-out for Atg5 (U2OS GFP-LC3 *Atg5*$^{-/-}$) were validated by immunoblot (A). U2OS GFP-LC3 and U2OS GFP-LC3 *Atg5*$^{-/-}$ were treated for 8 hours with lidocaine (Lido, 4 mM), ropivacaine (Ropi, 2 mM), levobupivacaine (Levo, 1 mM), bupivacaine (Bupi, 1 mM), prilocaine (Prilo, 4 mM), chloroprocaine (Chloro, 3 mM), rapamycin (Rapa, 30 µM). Autophagy was measured by assessing the GFP-LC3 dots surface by fluorescence microscopy. Data are depicted as representative images (B, scale bar equals 10 µm), bar chart (C), representative immunoblot (D) and densitometry data (n=3) (E). Data information: data were normalized to untreated condition for each cell line. Data are represented as the mean±SEM of three independent experiments. (C) Statistics were calculated using pairwise multiple comparison with a Benjamin-Hochberg correction. Stars indicate the *p* value of each treatment compared with the untreated condition for each cell line. Hashes indicate *p* value of knock-out cells compared with the wild-type cells for the same treatment. (E) Samples were compared with Student's *t*-test. *P<0.05, ***/###p<0.001.

antibody and fluorescence microscopy (figure 2A,B). Upon knock-in mutation of eIF2α to replace serine 51 by a non-phosphorylable alanine residue (eIF2α^{S51A}) (figure 2C), the induction of local anesthetic-induced RFP-LC3 *puncta* was blocked (figure 2D,E). However, the phosphorylation of eIF2α by local anesthetics was not

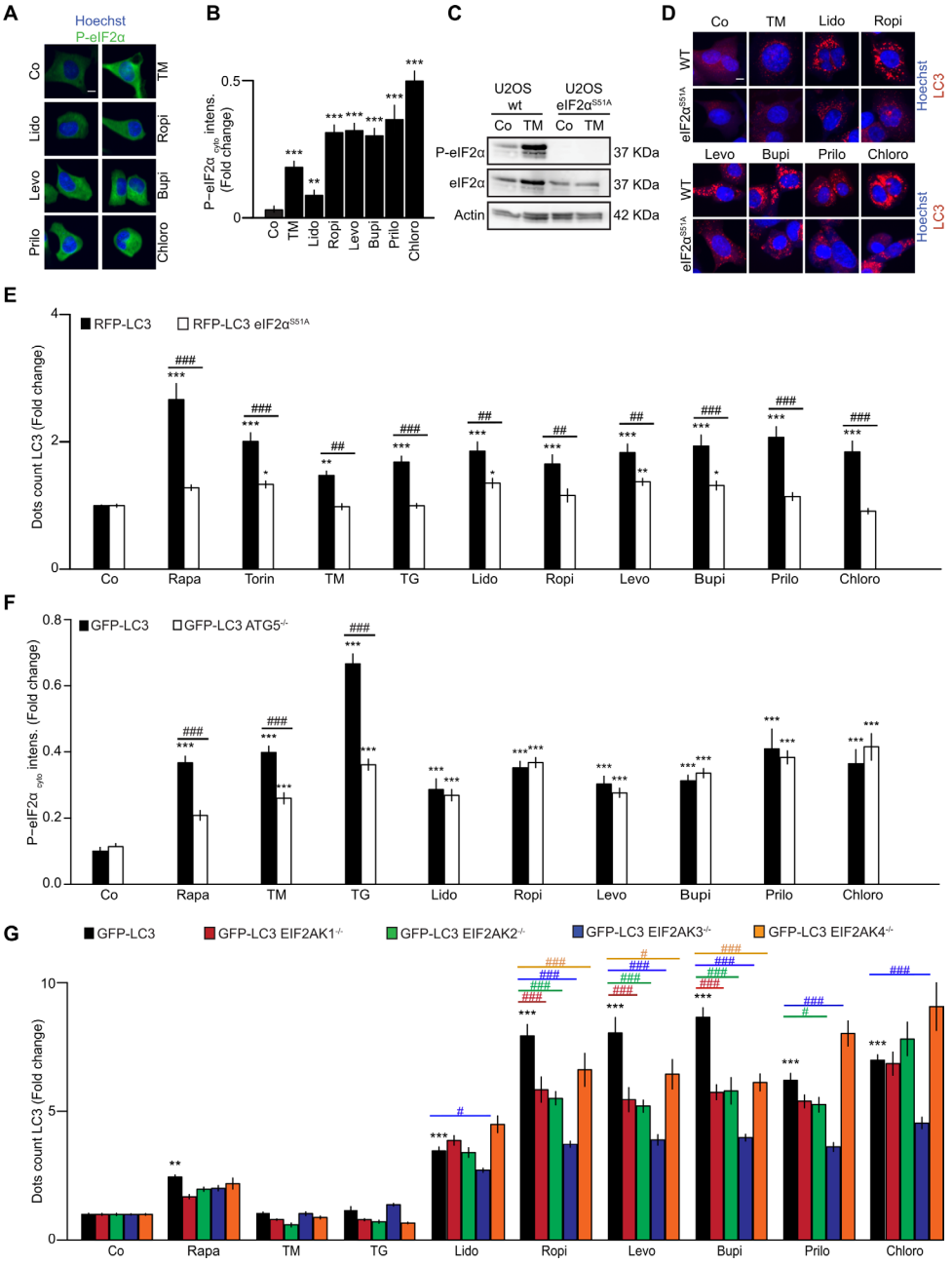

Figure 2 Induction of autophagy and endoplasmic reticulum stress depends on EIF2AK3 mediated phosphorylation of eIF2α A-G. U2OS wild-type cells were treated for 6 hours with lidocaine (Lido, 4 mM), ropivacaine (Ropi, 2 mM), levobupivacaine (Levo, 1 mM), bupivacaine (Bupi, 1 mM), prilocaine (Prilo, 4 mM), chloroprocaine (Chloro, 3 mM), tunicamycin (TM, 5 µM). eIF2α phosphorylation was measured by means of immunofluorescence staining using a phosphoneoepitope-specific antibody. Data are depicted as representative images (A, scale bar 10 µm), and representative bar charts (B). Human osteosarcoma U2OS wild-type cells, U2OS RFP-LC3 cells bearing a mutant non-phosphorylable version of eIF2α (U2OS eIF2α^{S51A}) were validated by immunoblot (C). U2OS cells stably expressing RFP-LC3, U2OS RFP-LC3 eIF2α^{S51A}, U2OS cells stably expressing GFP-LC3, U2OS GFP-LC3 knock-out for Atg5 (U2OS GFP-LC3 *Atg5*$^{-/-}$) and U2OS GFP-LC3 cells eIF2A knock-out for the kinases 1,2,3, and 4 were treated for 6 hours with lidocaine (Lido, 4 mM), ropivacaine (Ropi, 2 mM), levobupivacaine (Levo, 1 mM), bupivacaine (Bupi, 1 mM), prilocaine (Prilo, 4 mM), chloroprocaine (Chloro, 3 mM), tunicamycin (TM, 5 µM), thapsigargin (TG, 5 µM), rapamycin (Rapa, 30 µM), torin 1 (Torin, 300 nM). Autophagy was measured by assessing the LC3 dots surface using fluorescence microscopy (D, E, G). eIF2α phosphorylation was measured by means of immunofluorescence staining using a phosphoneoepitope-specific antibody (F). Data is depicted as representative images (scale bar equals 10 µm) and bar chart. (B, E, F and G) Data information: data were normalized to untreated condition for each cell line. Data are represented as the mean±SEM of three independent experiments. (B) Samples were compared with Student's *t*-test. (E, F and G) Statistics were calculated using pairwise multiple comparison with a Benjamin-Hochberg correction. (E, F) Stars indicate the *p* value of each treatment compared with untreated condition for each cell line. (G) Stars indicate the *p* value of each treatment compared with untreated condition of the wild-type cells. (E, F and G) Hashes indicate *p* value of knock-in cells or knock-out cells compared with the wild-type cells for the same treatment. $^{*/\#}$P<0.05, $^{**/\#\#}$p<0.01, $^{***/\#\#\#}$p<0.001.

decreased in *Atg5*$^{-/-}$ cells (figure 2F), and cell loss was attenuated in *Atg5*$^{-/-}$ cells as well (online supplemental figure S3). Collectively, these data suggest that local anesthetics induce cell death by a pathway that involves intertwined autophagic and ER stress responses. eIF2α is phosphorylated by four different eIF2α kinases (EIF2AK1 to EIF2AK4).[50] We determined the effects of the knock-out of each of these kinases (online supplemental figure S4A) on autophagy. The knock-out of EIF2AK3 had the strongest inhibitory effects on this parameter induced by local anesthetics (figure 2G), in line with the fact that this kinase (best known as PERK) is strongly tied to ER stress[51] . Local anesthetics also induced other signs of ER stress detectable with suitable biosensor cell lines, such as a cell line in which GFP is placed under the control of the ATF4 promoter (and that measures the translational activation of ATF4 expression downstream of eIF2α phosphorylation) (online supplemental figure S5A, B), the expression of a XBP1ΔDBD-venus fusion protein that is only in-frame for venus (a variant of GFP) when XBP1 has been spliced by IRE1 (online supplemental figure S5C, D), and the redistribution of a GFP-ATF6 fusion protein to the Golgi apparatus and the nucleus (online supplemental figure S5E, F).

In conclusion, local anesthetics trigger the activation of all three arms of the ER stress response, namely, EIF2AK3/PERK-dependent eIF2α phosphorylation leading to ATF4 translation, IRE1-mediated XBP1 activation, as well as activation of the latent transcription factor ATF6. The PERK-dependent phosphorylation of eIF2α is required for the induction of autophagy.

Autophagy-dependent and immune-dependent anticancer effects of local anesthetics

In the next step, we evaluated the anticancer effects of local anesthetics at clinically relevant concentrations on three different cancer types developing in immunocompetent mice, namely, cutaneous MCA205 fibrosarcomas, E0771 breast cancers and MC38 colon cancers. Lidocaine or ropivacaine significantly ($p<0.05$) inhibited the growth of all these cancers or increased the overall survival of mice (figure 3A–F). When combined with PD-1 blockade, additive effects were observed in several cases, for instance for ropivacaine +anti-PD-1 against MCA205 (figure 3B), as well as for lidocaine or ropivacaine +anti-PD-1 against MC38 (figure 3E and F). Importantly, the tumor growth-reducing and survival-extending effects of ropivacaine (figure 4) and all other local anesthetics (online supplemental figure S6) against MCA205 fibrosarcoma were only observed in immunocompetent wild type mice (figure 4A, online supplemental figure S6A) but were lost in *nu/nu* mice that lack mature T lymphocytes due to inborn athymia (figure 4B, online supplemental figure S6B). Moreover, MCA205 cells engineered to lose EIF2AK3/PERK (by CRISPR/Cas9 technology)[52] or ATG5 (by means of an SH-RNA-mediated knockdown)[13] and inoculated into immunocompetent wild-type mice formed tumors that were resistant against the anticancer effect of ropivacaine (figure 4C and D, online supplemental figure S4B). In the same way, the lack of PERK or ATG5 confers a cytoprotective effect on tumor cells after treatment *in vitro* with local anesthetics suggesting that ER stress and autophagy are both mechanisms implicated in the antitumor response induced by local anesthetics (online supplemental figures S7, S8A-C). When added to cultured cancer cells, local anesthetics induced the immunostimulatory release of ATP (which is autophagy-dependent)[13] (figure 4E) and HMGB1 (which is cell death-related)[15] (figure 4F), but failed to stimulate CALR exposure (which is linked to the integrated stress response but suppressed by the IRE1/XBP1 pathway) (figure 4G)[9 11 14 53] . Accordingly, local injection of recombinant CALR protein together with ropivacaine into orthotopic MCA205 fibrosarcomas enhanced the survival of mice more efficiently than the injection of CALR or ropivacaine alone (figure 4H). Moreover, tumors designed to overexpress the ecto-ATPase CD39, which destroys extracellular ATP, were unable to respond to local anesthetics (online supplemental figure S9).

Next, we investigate the immunogenic properties of local anesthetics. After treatment *in vitro,* MCA205 cells were labeled with CellTracker Orange (CMTMR) and their engulfment by bone marrow-derived CD11c^{+} dendritic cells (BMDCs) was assessed. Local anesthetics induced phagocytosis (figure 5A, online supplemental figure S10). Accordingly, local anesthetics elicited signs of an immune response *in vivo* by increasing CD4^{+} T lymphocytes, as well as the ratio of CD8^{+} T lymphocytes over FoxP3^{+}CD4^{+} T regulatory cells (Tregs) in the tumor immune infiltrate. Moreover, local anesthetics caused intratumoral CD8^{+} T cells to upregulate glucocorticoid-induced TNFR-related receptor (GITR) and inducible costimulatory (ICOS) (figure 5B–F).

Immunogenic cell death inducers have been reported to induce apoptosis, necroptosis or ferroptosis and to frequently inhibit DNA-to-RNA transcription.[54] Further results showed z-VAD-fmk and ferrostatin, which are inhibitors of pro-apoptotic caspases and ferroptosis, respectively failed to inhibit tumor cell death induced by local anesthetics. In contrast, necrostatin-1 attenuated the cytotoxic effects of lidocaine on tumor cells suggesting local anesthetics induce necroptosis (online supplemental figure S8D). Moreover, local anesthetics failed to inhibit transcription (online supplemental figure S11).

Altogether, these results suggest that local anesthetics can exert anticancer effects through a unique pathway that depends on the induction of autophagy in tumor cells as well as the presence of an intact immune system, but can be improved by the co-injection of CALR protein.

Inhibition of oxidative phosphorylation by local anesthetics has autophagy-dependent anticancer effects

Several reports indicate that local anesthetics can cause an inhibition of oxidative phosphorylation in different cell types including neurons, chondrocytes and cardiomyocytes.[55–58] Therefore, we determined the capacity of

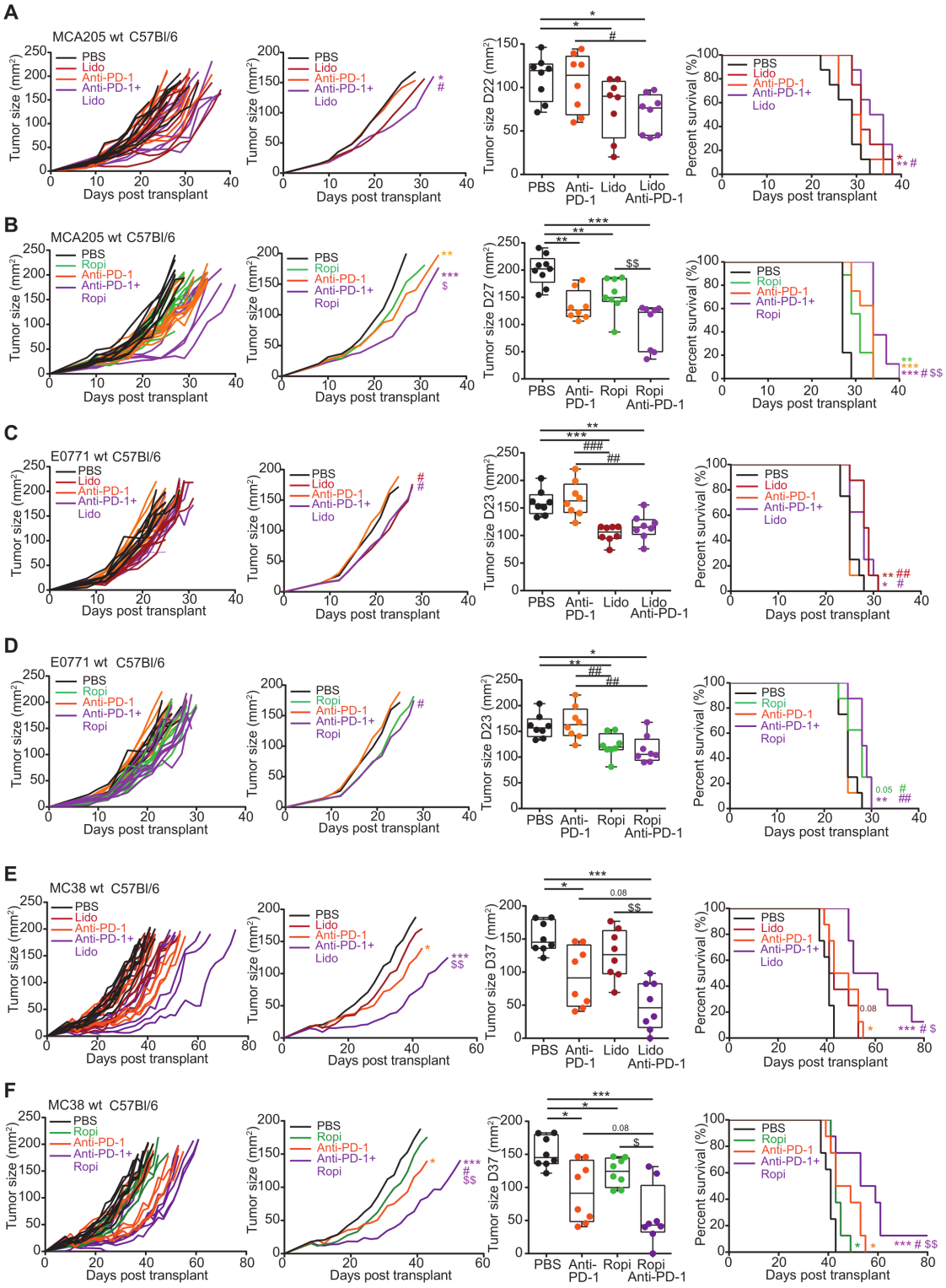

Figure 3 Lidocaine and ropivacaine foster anticancer effects that are potentiated by immunotherapy A–F. Murine fibrosarcoma MCA205 (A, B), breast cancer E0771 (C, D) or colon adenocarcinoma MC38 cells (E, F) were injected subcutaneously (*s.c.*) into the flank of immunocompetent C57BL/6 mice with 8 mice per group (n=9 for PBS and ropivacaine (Ropi) (B)). When tumors became palpable, mice were treated for 2 days by intratumoral injections of PBS as control (PBS), lidocaine (Lido, 3 mg/kg) or Ropi (4 mg/kg). Anti-PD-1 intraperitoneal injections were performed at days 8, 12 and 16 after injection of local anesthetics. Data information: Figures C and D provide from the same experiment. PBS and anti-PD-1 groups are the same in both figures. Figures E and F provide from the same experiment. PBS and anti-PD-1 groups are the same in both figures. Tumor size comparison was calculated using a type II analysis of variance (ANOVA) test and pairwise Wilcoxon test. Data are represented as boxplot. Overall survival was compared with a log-rank test. *P<0.05, **p<0.01, ***p<0.001, compared with controlled mice, #p<0.05, ##p<0.01, ###p<0.001, compared with anti-PD-1-alone-treated mice and $p<0.05, $$p<0.01, $$$p<0.001, compared with local anesthetic-alone-treated mice.

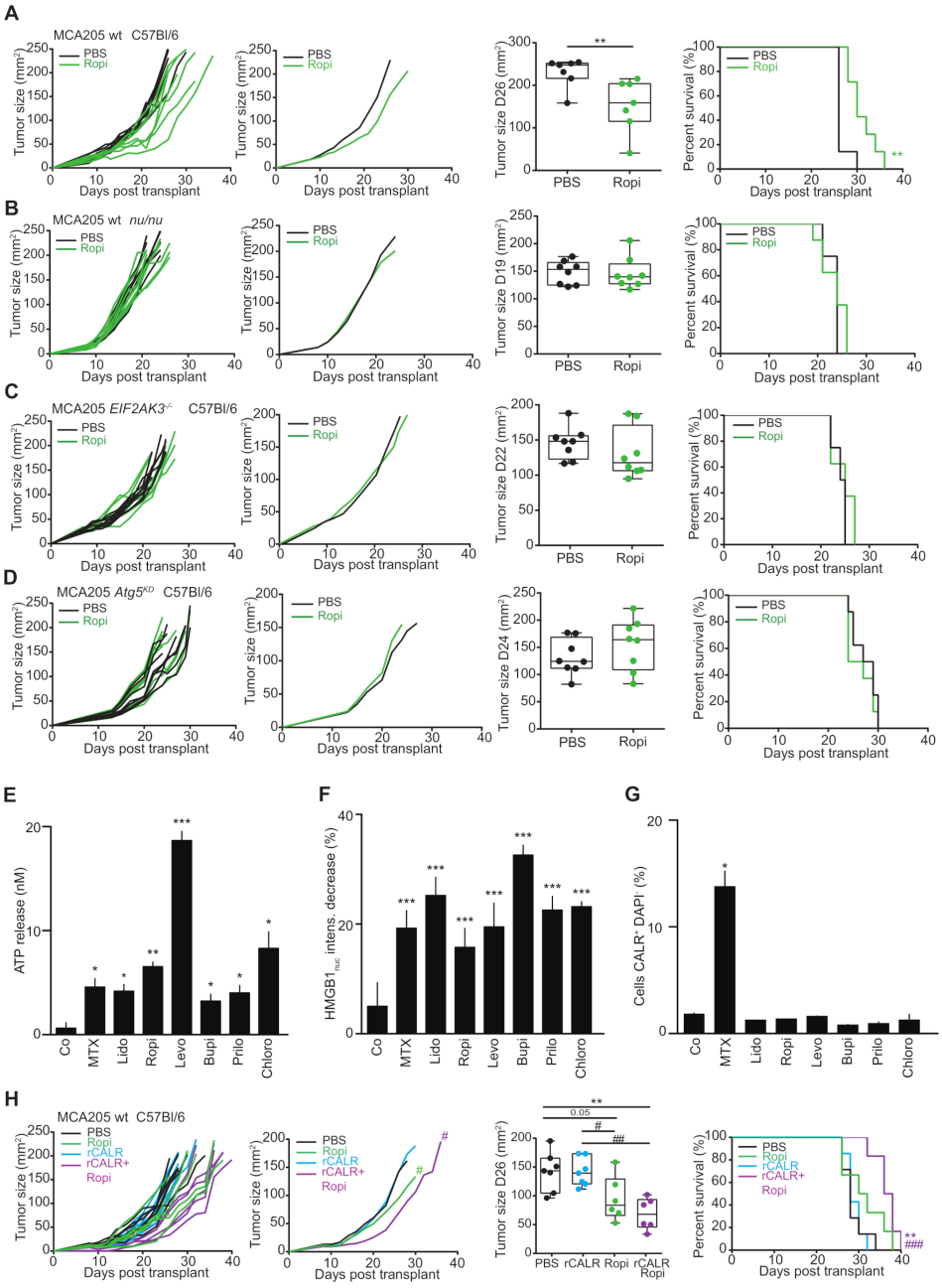

Figure 4 Local anesthetics promote antitumor immune responses mediated by premortem stress and traits of immunogenic cell death A–H**.** (A–D) Murine fibrosarcoma MCA205 cells were injected subcutaneously (*s.c.*) into the flank of immunocompetent C57BL/6 mice (A) with 7 mice per group and of immunodeficient *nu/nu* mice (B) with 8 mice per group. MCA205 *EIF2AK3*$^{-/-}$ and MCA205 *Atg5*^{KD} cells were injected *s.c.* into the flank of immunocompetent C57BL/6 mice with 8 mice per group (C, D). When tumors became palpable, mice were treated for 2 days by intratumoral (*i.t.*) injections of PBS as control (PBS) or ropivacaine (Ropi, 4 mg/kg). (E–G) Human osteosarcoma U2OS wild-type cells and U2OS cells stably expressing HMGB1-GFP were treated for 24 hours (E, F) or 6 hours (G) with lidocaine (Lido, 5 mM), Ropi (6 mM), levobupivacaine (Levo, 3 mM), bupivacaine (Bupi, 1 mM), prilocaine (Prilo, 4 mM), chloroprocaine (Chloro, 4 mM), mitoxantrone (MTX, 3 µM) (E) or with Lido (4 mM), Ropi (2 mM), Levo (1 mM), Bupi (1 mM), Prilo (4 mM), Chloro (3 mM), MTX (3 µM) (F, G). Adenosine triphosphate (ATP) release was assessed by bioluminescence (E) HMGB1 release was assessed by measuring GFP fluorescence decrease by fluorescence microscopy (F). Calreticulin (CALR) exposure was determined by immunofluorescence staining and flow cytometry. Data are expressed as the percentage of CALR positive, diamidino-2- phenylindole (DAPI) negative ($CALR^+$ $DAPI^-$) cells (G). MCA205 cells were injected *s.c.* into the flank of immunocompetent C57BL/6 mice with 7 mice per group (n=6 for Ropi and rCALR +Ropi). When tumors became palpable, mice were treated for 2 days by *i.t.* injections of PBS or Ropi (4 mg/kg) or recombinant CALR (rCALR, 15 µg) or Ropi (4 mg/kg) supplemented with recombinant calreticulin (rCALR, 15 µg) (H). Data information: *In vitro,* data are represented as the mean±SD of one experiment representative of three independent experiments. Samples were compared with Student's *t*-test. *P<0.05, **p<0.01, ***p<0.001. *In vivo*, mean tumor size was compared using a type II analysis of variance (ANOVA) test and pairwise Wilcoxon test. Data are represented as boxplots. Overall survival was compared with a log-rank test. *P<0.05, **p<0.01, ***p<0.001, compared with controlled mice, #p<0.05, ##p<0.01, ###p<0.001, compared with rCALR-alone-treated mice.

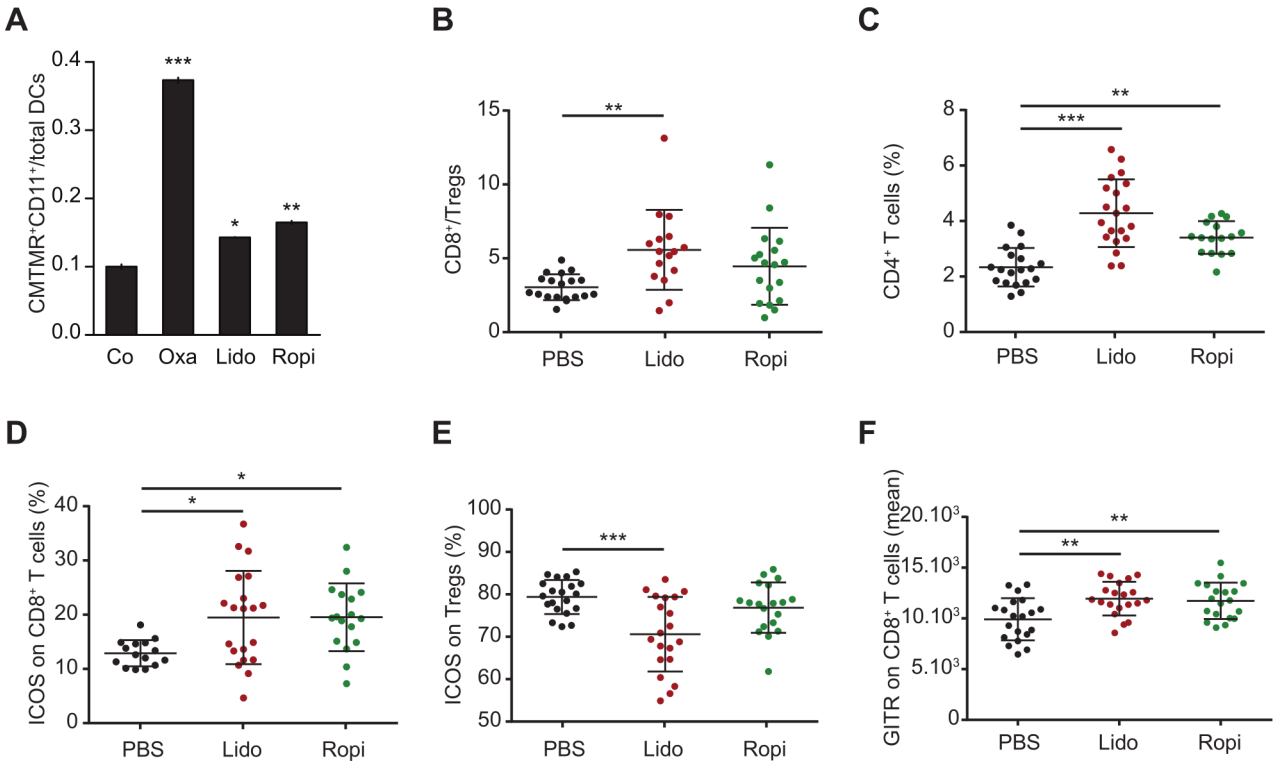

Figure 5 Local anesthetics induce phagocytosis and modulate tumor-infiltrating lymphoid cell subsets A–F. Murine fibrosarcoma MCA205 cells were stained with CellTracker orange (CMTMR$^+$) for 30 min and treated for 24 hours with lidocaine (Lido, 6 mM), ropivacaine (Ropi, 4 mM) or oxaliplatin (Oxa, 500 µM). Then, cells were co-cultured with differentiated bone marrow-derived dendritic cells for 4 hours at 37°C. Dendritic cells (DCs) were determined by immunostaining using a CD11c-specific antibody (CD11c-APC). Data are represented as the mean±SD of one representative of two independent experiments. Samples were compared with Student's *t*-test. *P<0.05, **p<0.01, ***p<0.001 (A). Murine fibrosarcoma MCA205 wild-type cells were injected *s.c.* into the flank of immunocompetent C57BL/6 mice with 20 mice per group (19 mice in Ropi group). When tumors became palpable, mice were treated for 2 days by intratumoral (*i.t.*) injections of PBS as control (PBS), lidocaine (Lido, 3 mg/kg) or ropivacaine (Ropi, 4 mg/kg). Mice were sacrificed at day 9. Tumors were collected and T cell populations infiltrating the tumor were analyzed by immunostaining and flow cytometry (B–C). Level of expression of ICOS at the surface of CD8$^+$ T cells and T regulator cells as well as level of expression of glucocorticoid-induced TNFR-related protein (GITR) at the surface of CD8$^+$ T cells were depicted (D–F). Samples were compared using a one-way analysis of variance (ANOVA), Tukey's multiple comparisons test. Outliers were excluded based on the ROUT test (Q=10%, test combining robust regression and outlier removal). Data are depicted as mean±SD. *P<0.05, **p<0.01, ***p<0.001 (B–F).

different local anesthetics to inhibit oxygen consumption by U2OS cells. When added to cells that are in a state of maximal respiration (due to the addition of the uncoupling agent carbonylcyanide-3-chlorophenylhydrazone, CCCP), the addition of the six different local anesthetics (used at the IC_{20}) caused an immediate reduction of oxygen consumption that was as efficient as that caused by the positive control rotenone, an inhibitor of respiratory chain complex I (figure 6A). Moreover, preincubation of cells with each of the six local anesthetics for 6 hours reduced basal respiration, which could be partially increased by addition of CCCP, but then was further inhibited by rotenone (figure 6B). This regimen of preincubation with local anesthetics enhanced basal glycolysis (as determined by the extracellular acidification rate, ECAR, reflecting lactate accumulation) that was not further increased by inhibition of oxidative phosphorylation by oligomycin (figure 6C). Of note, when added to U2OS cells expressing a mitochondrion-targeted dsRED biosensor, local anesthetics and mitochondrial inhibitors including CCCP, carbonylcyanide-4-trifluoromethoxyphenylhydrazone (FCCP) and rotenone indistinguishably induced progressive rounding up of mitochondria, as determined by video fluorescence microscopy (figure 6D and E). These results suggest that local anesthetics alter cellular metabolism by inhibiting oxidative phosphorylation. We therefore examined the possibility that mitochondrial inhibitors would induce a similar pattern of stress responses as local anesthetics. CCCP (but less for rotenone) stimulated the formation of GFP-LC3 *puncta* (figure 6F and G). Both CCCP and rotenone caused the immunofluorescence-detectable phosphorylation of eIF2α (figure 6H and I) and the redistribution of FYVE-RFP to dots (online supplemental figure S12A, B). CCCP induced the activation of the three arms of the ER stress response, while rotenone only induced ATF4 and XBP1 activation, not that of ATF6 (online supplemental figure S12C-H). Rotenone was also able to activate the three hallmarks of immunogenic cell death (ATP release, CALR exposure, HMGB1 exodus), while CCCP only

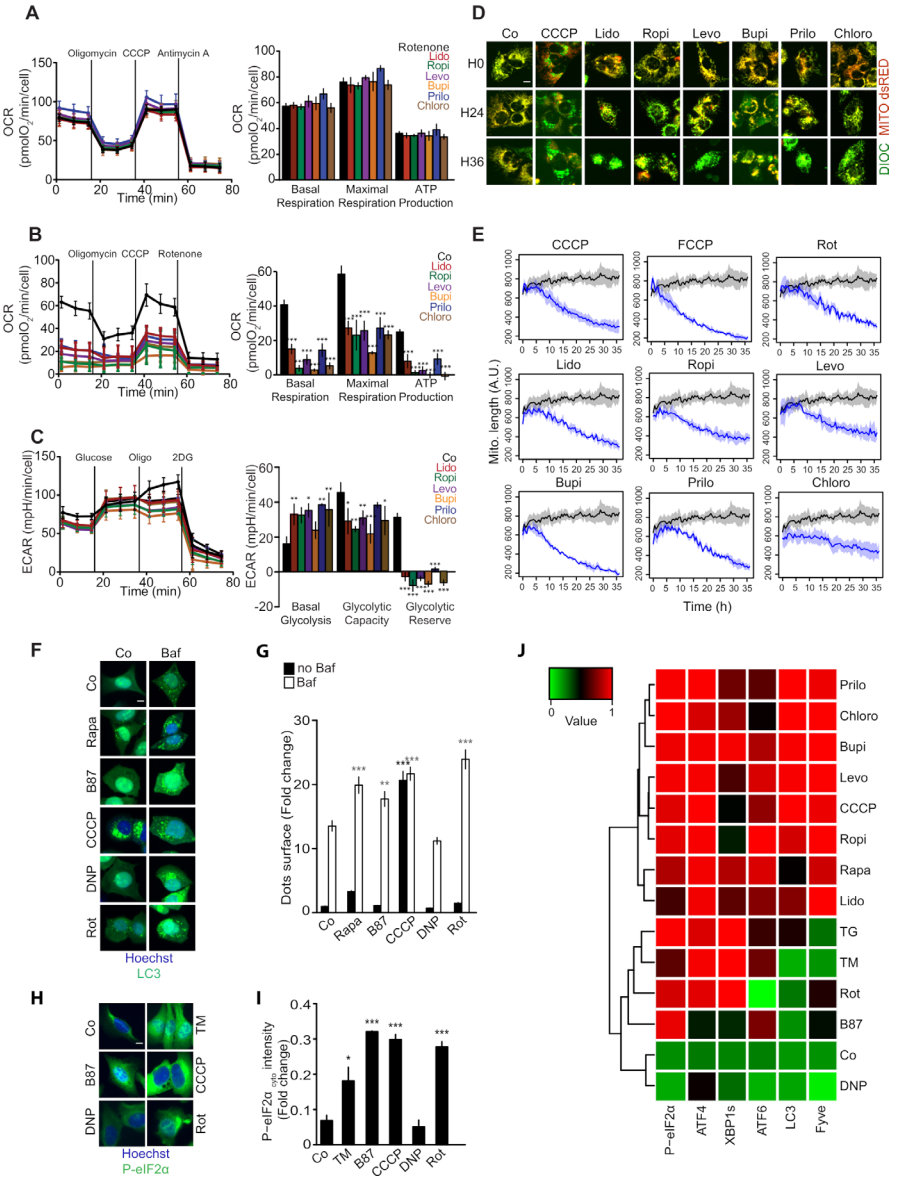

Figure 6 Local anesthetics induce mitochondrial toxicity mimicking mitochondrial uncouplers A–J. (A–E) U2OS cells were treated with lidocaine (Lido, 4 mM), ropivacaine (Ropi, 2 mM), levobupivacaine (Levo, 1 mM), bupivacaine (Bupi, 1 mM), prilocaine (Prilo, 4 mM), chloroprocaine (Chloro, 3 mM). Oxygen consumption rate (OCR) of U2OS wild-type cells was measured by means of a Seahorse analyzer with the replacement of rotenone injection by local anesthetics (A). Furthermore, cells were analyzed after 6 hours of treatment with local anesthetics to assess OCR (B) and the extracellular acidification rate (ECAR) (C). Results are expressed as mean±SD of one experiment representative of three independent experiments. U2OS cells stably expressing MITOdsRED were treated for 36 hours. Viability (DIOC) and mitochondrial fiber length (MITOdsRED) were visualized by fluorescence microscopy (D) and quantified (black curve: untreated cells; blue curve: treated cells) (E). Human osteosarcoma U2OS wild-type and U2OS GFP-LC3 cells were treated with rapamycin (Rapa, 30 µM), respiratory chain complex I inhibitor BAY87-2243 (B87, 50 µM), carbonyl cyanide m-chloro-phenyl hydrazone (CCCP, 50 µM), 2,4-dinitrophenol (DNP, 50 µM), rotenone (Rot, 50 µM), bafilomycin (Baf, 100 nM). Autophagy was assessed after 8 hours of treatment by analyzing the dots surface of GFP-LC3 *puncta*. Data are depicted as representative images and bar charts (F, G). eIF2α phosphorylation was assessed after 6 hours of treatment by analyzing immunofluorescence staining using a phosphoneoepitope-specific antibody and the increase in cytoplasmic signal intensity was depicted as representative images and bar chart. Results are expressed as mean±SEM (n=3) (H, I). Human osteosarcoma U2OS wild-type cells and U2OS cells stably expressing pSMALB-ATF4.5rep, XBP1ΔDBD-venus-RFP-FYVE, GFP-ATF6 or GFP-LC3 were treated with lidocaine (Lido, 5 mM), ropivacaine (Ropi, 3 mM), levobupivacaine (Levo, 1 mM), bupivacaine (Bupi, 1 mM), prilocaine (Prilo, 4 mM), chloroprocaine (Chloro, 4 mM), rapamycin (Rapa, 30 µM), B87 (50 µM), CCCP, (50 µM), DNP (50 µM), Rot (50 µM) for 6 hours, 12 hours, 12 hours, 6 hours and 8 hours, respectively. Data are arranged as a heatmap as indicated by the color scale. Raw data were normalized with a sigmoidal scaling, n=3 (J). Data information: data were normalized to untreated condition. (G) Statistics were calculated using pairwise multiple comparison with a Benjamin-Hochberg correction. Stars indicate the *p* value of each treatment compared with untreated condition (black stars) or compared with bafilomycin condition (grey stars). (I) Samples were compared with Student's t-test. *P<0.05, **p<0.01, ***p<0.001.

translocated calreticulin at the plasma membrane and activated the release of HMGB1 (online supplemental figure S13A-C). Nonhierarchical clustering analysis of all these cellular effects indicated that local anesthetics induce a pattern of ER- and autophagy-related stress responses that most closely resembles those elicited by the uncoupler CCCP (figure 6J). In sum, local anesthetics perturb mitochondrial morphology and function as they induce cellular stress responses similar to those caused by CCCP.

Driven by these findings, we evaluated the possible anticancer effects of CCCP and its analog FCCP on fibrosarcomas, mammary carcinomas and colon cancers developing in immunocompetent mice. Local injection of CCCP and FCCP caused tumor growth reduction that in several instances, in particular in MCA205 and MC38 cancers, was additive with the effects of PD-1 blockade (online supplemental figure S14). Again, tumor growth reduction by CCCP was lost when relevant stress pathways were blocked in the tumor cells by knock-out of PERK or knockdown of ATG5 (figure 7A–C), but was enhanced by local injection of recombinant CALR protein (figure 7D). Thus, CCCP apparently compromises tumor growth through mechanisms that resemble those triggered by local anesthetics.

DISCUSSION

In this paper, we report that the six most widely used local anesthetics can trigger T lymphocyte-dependent tumor growth reduction that is variably improved by systemic administration of anti-PD-1 antibodies or local injection of CALR, but lost upon genetic inhibition of the integrated stress response (the EIF2AK3/PERK-dependent phosphorylation of eIF2α) and autophagy. Mechanistically, local anesthetics induce the integrated stress response (with activation of the ER stress-relevant kinase EIF2AK3/PERK, leading to the phosphorylation of eIF2α) which is required for the induction of autophagy.[48] In addition, local anesthetics stimulate a full-blown ER stress response with activation of the transcription factors ATF4, XBP1 and ATF6. Although EIF2AK3/PERK-catalyzed eIF2α phosphorylation is required for CALR exposure,[14] the activation of the IRE1/XBP1 arm of the ER stress response suppresses CALR exposure,[9 53] explaining the net result that local anesthetics fail to stimulate the translocation of CALR from the ER lumen to the cell surface. However, local anesthetics were able to elicit other immunostimulatory stress signals including the release of ATP and HMGB1 from cancer cells, likely explaining their immune effects. Taken together, these data suggest that the administration of a local anesthetic into a (still immunologically 'cold' tumor) causes local stress, the stress response lasting longer than the presence of the drug, hence setting of a cascade that ignites the recruitment of immune effectors and renders the tumor immunologically 'hot'.

Of note, reportedly local anesthetics induce various modalities of cell stress and death (autophagy, apoptosis, necrosis…) in a time-and dose-dependent fashion, as previously described to explain their neurotoxicity.[59 60] In line with the literature,[61] the use of specific caspase inhibitor such as z-VAD-fmk failed to interfere with tumor cell death mediated by local anesthetics. Toxicities of local anesthetics may involve damage of cell membranes and mitochondria. Thus, local anesthetics inhibit oxidative phosphorylation and perturb mitochondrial morphology in cultured cancer cells, in line with previous observation suggesting uncoupling effects on mitochondria from normal cells.[55–58] The mitochondrial uncoupler CCCP fully mimicked the cell stress-inducing and immune-dependent anticancer effects of local anesthetics at all levels, including the stimulation of autophagy, all arms of the ER stress response and two hallmarks of ICD. Moreover, local injection of CCCP or that of its close structural and functional analog FCCP had anticancer effect that required EIF2AK3/PERK and ATG5 expression by the tumor cells. Altogether, these results can be interpreted to mean that the bioenergetic effects of local anesthetics are responsible for their immunostimulatory function. Although long-term uncoupling effects would probably compromise the function of tumor-infiltrating immune cells,[62] the transient presence of locally injected anesthetics (and presumably CCCP and FCCP as well) appears to be compatible with immune effector functions as demonstrated by the induction of tumor cell phagocytosis by immature dendritic cells induced *in vitro* and the signs of a T cell-mediated anticancer immune response observable within tumors.[63]

Irrespective of the exact mechanisms that account for the pro-immunosurveillance effects of local anesthetics, there is ample clinical evidence in favor of anticancer effects of such compounds. Indeed, several retrospective clinical trials observed a decrease in recurrence and a better survival after local anesthetics injection alone or in supplement of general anesthesia during solid tumor resection.[64–70] A meta-analysis conducted on 21 studies supported a positive association between local anesthetics and oncological outcomes compared with general anesthesia (overall survival p=0.026; recurrence free survival p=0.047).[71] Thus, local anesthesia performed for tumor biopsies, for melanoma exeresis, regional block anesthesia (such as block of the axillary brachial plexus, serratus anterior plane, or pectoralis nerve) realized in the context of tumorectomy and lymphadenectomy, may directly induce immunogenic stress in cancer cells. In addition, local anesthetics injected close to the tumor site might reduce the migration of residual malignant cells released during surgery. Whether these effects are solely due to activation of immunogenic stress or rather involve additional effects such as the well-studied anti-inflammatory effects of local anesthetics or the direct activation of natural killer cells remains an open question.[63 72 73]

The most important limitation of this study resides in its preclinical nature, requiring validation at the clinical level.

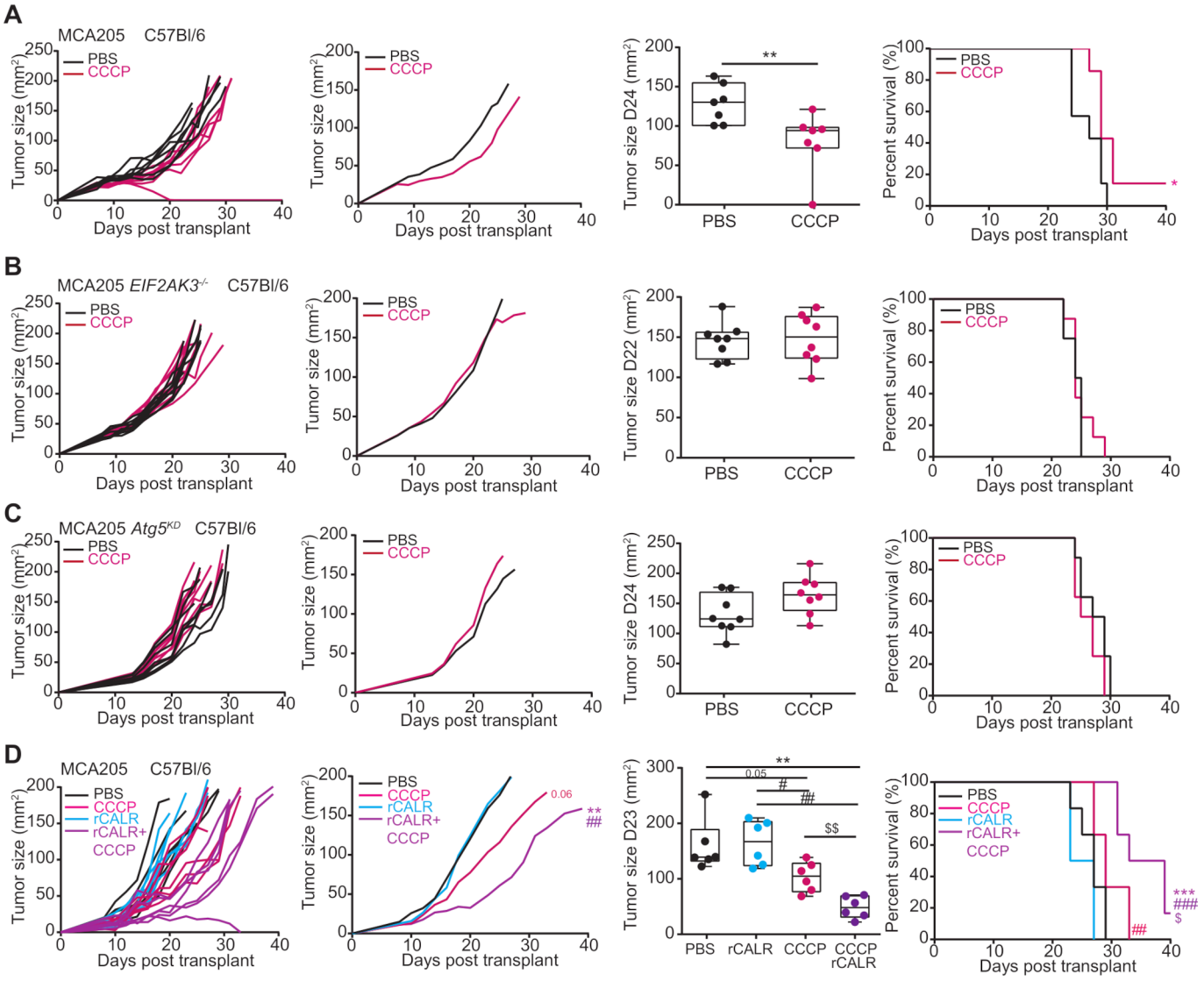

Figure 7 Mitochondrial uncouplers mimic local anesthetics and promote antitumor immune responses mediated by premortem stress A–D. Murine fibrosarcoma MCA205 cells were injected subcutaneously (*s.c.*) into the flank of immunocompetent C57BL/6 mice with 7 mice per group (A). MCA205 *EIF2AK3*$^{-/-}$ cells were injected *s.c.* into the flank of immunocompetent C57BL/6 mice with 8 mice per group (B). MCA205 *Atg5*^{KD} cells were injected *s.c.* into the flank of immunocompetent C57BL/6 mice with 8 mice per group (C). When tumors became palpable, mice were treated for 2 days by intratumoral (*i.t.*) injections of PBS as control (PBS) or CCCP (0.25 mg/kg). (D) MCA205 cells were injected *s.c.* into the flank of immunocompetent C57BL/6 mice with 6 mice per group. When tumors became palpable, mice were treated for 2 days by *i.t.* injections of PBS as control (PBS), CCCP (0.25 mg/kg) or recombinant calreticulin (rCALR, 15 µg) or CCCP (0.25 mg/kg)+rCALR (15 µg). Data information: figures 4C and 7B provide from the same experiment. PBS group are the same in these both figures. Figures 4D and 7C provide from the same experiment. PBS group are the same in these both figures. Mean tumor sizes were compared using a type II analysis of variance (ANOVA) test and pairwise Wilcoxon test. Data are represented as boxplots. Overall survival was compared with a log-rank test. *P<0.05, **p<0.01, ***p<0.001, compared with controlled mice, $^{\#}$p<0.05, $^{\#\#}$p<0.01, $^{\#\#\#}$p<0.001, compared with rCALR-single-treated mice and $^{\$}$p<0.05, $^{\$\$}$p<0.01, $^{\$\$\$}$p<0.001, compared with mitochondrial uncoupler-single-treated mice.

More than twenty prospective trials are currently evaluating the prognostic and immune effects of local anesthetics administered via distinct routes (intraperitoneal injection, spinal anesthesia, epidural anesthesia, infusion pumps…) to patients with multiple different cancer types (online supplemental table 1). The results of these studies may influence future guidelines in onco-anesthesia.

Author affiliations
[1]Equipe labellisée par la Ligue contre le cancer, Université de Paris Cité, Sorbonne Université, INSERM UMR1138, Centre de Recherche des Cordeliers, Paris, France
[2]Metabolomics and Cell Biology Platforms, Gustave Roussy Cancer Campus, Villejuif, France
[3]Anesthesiology Department, Gustave Roussy Cancer Campus, Villejuif, France
[4]Institute for Research in Immunology and Cancer (IRIC), Université de Montréal, Montreal, Québec, Canada
[5]Department of Medicine, Université de Montréal, Montreal, Québec, Canada
[6]Institut National de la Santé et de la Recherche Médicale, Unité 1151, Université de Paris Cité, Centre National de la Recherche Scientifique, UMR 8253, Paris, France
[7]Gustave Roussy, Villejuif, France
[8]Aix Marseille University, INSERM, CNRS, CRCM, Marseille, France
[9]Pôle de Biologie, Hôpital européen Georges Pompidou, AP-HP, Paris, France

Acknowledgements We are grateful to the support of the Gustave Roussy Cancer Campus, Université Paris-Saclay.

Contributors LB performed most experimental procedures, analyses, preparation of the manuscript and is responsible for the overall content as the guarantor. AWC performed HMGB1 video, oxygen consumption and glycolytic flux experiments and participated in autophagic experiments. AS helped in statistical analyses and image acquisition. JH generated eIF2αS51A cells as well as the knockout cells lacking EIF2A kinases 1-4. WX generated the MCA205 EIF2AK3 knockout cell line. GC performed the experiments of transcription. PL, LZ, SZ participated in phagocytosis experiments. JLN and JP participated in the characterization of the tumor immune infiltrate. PvE generated recombinant calreticulin. OK helped in figure design. FB provided intellectual input. GK and LB conceived and directed the project, and wrote the manuscript.

Funding GK is supported by the Ligue contre le Cancer (équipe labellisée); Agence Nationale de la Recherche (ANR)—Projets blancs; ANR under the frame of E-Rare-2, the ERA-Net for Research on Rare Diseases; Association pour la recherche sur le cancer (ARC); Cancéropôle Ile-de-France; Chancellerie des universités de Paris (Legs Poix), Fondation pour la Recherche Médicale (FRM); a donation by Elior; European Research Area Network on Cardiovascular Diseases (ERA-CVD, MINOTAUR); Gustave Roussy Odyssea, the European Union Horizon 2020 Project Oncobiome; Fondation Carrefour; High-end Foreign Expert Program in China (GDW20171100085 and GDW20181100051), Institut National du Cancer (INCa); Inserm (HTE); Institut Universitaire de France; LeDucq Foundation; the LabEx Immuno-Oncology; the RHU Torino Lumière; the Seerave Foundation; the SIRIC Stratified Oncology Cell DNA Repair and Tumor Immune Elimination (SOCRATE); and the SIRIC Cancer Research and Personalized Medicine (CARPEM). LB is supported by Bristol-Myers-Squibb (BMS). Foundation for Research in Immuno-Oncology. AWC was supported by El Programa Nacional de Becas 'Don Carlos Antonio Lopez' (BECAL). JH was supported by the Philanthropia Foundation. WX and SZ received support by the China scholarship council. PvE acknowledges support by the Fondation pour la Recherche Médicale (EQU201903007853).

Competing interests GK and OK are cofounders of Samsara Therapeutics. JP is the inventor of patents for cancer vaccination licensed to Turnstone Biologics.

Patient consent for publication Not applicable.

Ethics approval All mice experiments were conducted according to EU Directive 63/2010 with the following protocols approved by the Ethical committee of the Gustave Roussy Cancer Campus (CEEA IRCIV/IGR no.26, registered at the French Ministry of Research, (2018100208217977v3; 2020070716191430v2; 2020100809149728v2; and 2021061408119739v2).

Provenance and peer review Not commissioned; externally peer reviewed.

Data availability statement Data are available on reasonable request.

ORCID iDs
Lucillia Bezu http://orcid.org/0000-0002-3569-6066
Wei Xie http://orcid.org/0000-0001-5554-2075
Jonathan Pol http://orcid.org/0000-0002-8355-7562
Oliver Kepp http://orcid.org/0000-0002-6081-9558

REFERENCES

1 Hanahan D, Weinberg RA. Hallmarks of cancer: the next generation. *Cell* 2011;144:646–74.
2 Schreiber RD, Old LJ, Smyth MJ. Cancer immunoediting: integrating immunity's roles in cancer suppression and promotion. *Science* 2011;331:1565–70.
3 Murciano-Goroff YR, Warner AB, Wolchok JD. The future of cancer immunotherapy: microenvironment-targeting combinations. *Cell Res* 2020;30:507–19.
4 Sharma P, Siddiqui BA, Anandhan S, *et al*. The next decade of immune checkpoint therapy. *Cancer Discov* 2021;11:838–57.
5 Krysko DV, Garg AD, Kaczmarek A, *et al*. Immunogenic cell death and DAMPs in cancer therapy. *Nat Rev Cancer* 2012;12:860–75.
6 Galluzzi L, Humeau J, Buqué A, *et al*. Immunostimulation with chemotherapy in the era of immune checkpoint inhibitors. *Nat Rev Clin Oncol* 2020;17:725–41.
7 Petroni G, Buqué A, Zitvogel L, *et al*. Immunomodulation by targeted anticancer agents. *Cancer Cell* 2021;39:310–45.
8 Obeid M, Tesniere A, Ghiringhelli F, *et al*. Calreticulin exposure dictates the immunogenicity of cancer cell death. *Nat Med* 2007;13:54–61.
9 Bezu L, Sauvat A, Humeau J, *et al*. eIF2α phosphorylation is pathognomonic for immunogenic cell death. *Cell Death Differ* 2018;25:1375–93.
10 Humeau J, Sauvat A, Cerrato G, *et al*. Inhibition of transcription by dactinomycin reveals a new characteristic of immunogenic cell stress. *EMBO Mol Med* 2020;12:e11622.
11 Humeau J, Bezu L, Kepp O, *et al*. EIF2α phosphorylation: a hallmark of both autophagy and immunogenic cell death. *Mol Cell Oncol* 2020;7:1776570.
12 Ghiringhelli F, Apetoh L, Tesniere A, *et al*. Activation of the NLRP3 inflammasome in dendritic cells induces IL-1beta-dependent adaptive immunity against tumors. *Nat Med* 2009;15:1170–8.
13 Michaud M, Martins I, Sukkurwala AQ, *et al*. Autophagy-Dependent anticancer immune responses induced by chemotherapeutic agents in mice. *Science* 2011;334:1573–7.
14 Panaretakis T, Kepp O, Brockmeier U, *et al*. Mechanisms of pre-apoptotic calreticulin exposure in immunogenic cell death. *Embo J* 2009;28:578–90.
15 Apetoh L, Ghiringhelli F, Tesniere A, *et al*. Toll-Like receptor 4-dependent contribution of the immune system to anticancer chemotherapy and radiotherapy. *Nat Med* 2007;13:1050–9.
16 Yang H, Xia L, Chen J, *et al*. Stress-glucocorticoid-TSC22D3 axis compromises therapy-induced antitumor immunity. *Nat Med* 2019;25:1428–41.
17 McKee AM, Kirkup BM, Madgwick M, *et al*. Antibiotic-induced disturbances of the gut microbiota result in accelerated breast tumor growth. *iScience* 2021;24:103012.
18 Angrish MD, Agha A, Pezo RC. Association of antibiotics and other drugs with clinical outcomes in metastatic melanoma patients treated with immunotherapy. *J Skin Cancer* 2021;2021:1–5.
19 Khan U, Ho K, Hwang EK, *et al*. Impact of use of antibiotics on response to immune checkpoint inhibitors and tumor microenvironment. *Am J Clin Oncol* 2021;44:247–53.
20 Haldar R, Ricon-Becker I, Radin A, *et al*. Perioperative COX2 and β-adrenergic blockade improves biomarkers of tumor metastasis, immunity, and inflammation in colorectal cancer: A randomized controlled trial. *Cancer* 2020;126:3991–4001.
21 Wrobel LJ, Gayet-Ageron A, Le Gal F-A. Effects of beta-blockers on melanoma microenvironment and disease survival in human. *Cancers* 2020;12. doi:10.3390/cancers12051094. [Epub ahead of print: 28 04 2020].
22 Hiller JG, Cole SW, Crone EM, *et al*. Preoperative β-Blockade with propranolol reduces biomarkers of metastasis in breast cancer: a phase II randomized trial. *Clin Cancer Res* 2020;26:1803–11.
23 Alazawi W, Pirmadjid N, Lahiri R, *et al*. Inflammatory and immune responses to surgery and their clinical impact. *Ann Surg* 2016;264:73–80.
24 Sztwiertnia I, Schenz J, Bomans K, *et al*. Sevoflurane depletes macrophages from the melanoma microenvironment. *PLoS One* 2020;15:e0233789.
25 Jeon S, Kim H-K, Kwon J-Y, *et al*. Role of sevoflurane on natural killer group 2, member D-mediated immune response in non-small-cell lung cancer: an in vitro study. *Med Sci Monit* 2020;26:e926395.
26 Khabbazi S, Hassanshahi M, Hassanshahi A, *et al*. Opioids and matrix metalloproteinases: the influence of morphine on MMP-9 production and cancer progression. *Naunyn Schmiedebergs Arch Pharmacol* 2019;392:123–33.
27 Thaker PH, Han LY, Kamat AA, *et al*. Chronic stress promotes tumor growth and angiogenesis in a mouse model of ovarian carcinoma. *Nat Med* 2006;12:939–44.
28 Sood AK, Bhatty R, Kamat AA, *et al*. Stress hormone-mediated invasion of ovarian cancer cells. *Clin Cancer Res* 2006;12:369–75.

29 Wong HPS, Ho JWC, Koo MWL, *et al*. Effects of adrenaline in human colon adenocarcinoma HT-29 cells. *Life Sci* 2011;88:1108–12.
30 Ogawa K, Hirai M, Katsube T, *et al*. Suppression of cellular immunity by surgical stress. *Surgery* 2000;127:329–36.
31 Liu D, Sun X, Du Y, *et al*. Propofol promotes activity and tumor-killing ability of natural killer cells in peripheral blood of patients with colon cancer. *Med Sci Monit* 2018;24:6119–28.
32 Zhou M, Dai J, Zhou Y, *et al*. Propofol improves the function of natural killer cells from the peripheral blood of patients with esophageal squamous cell carcinoma. *Exp Ther Med* 2018;16:83–92.
33 Zhang Y-F, Li C-S, Zhou Y, *et al*. Effects of propofol on colon cancer metastasis through STAT3/HOTAIR axis by activating WIF-1 and suppressing Wnt pathway. *Cancer Med* 2020;9:1842–54.
34 Liu Z, Cheng S, Fu G, *et al*. Postoperative administration of ketorolac averts morphine-induced angiogenesis and metastasis in triple-negative breast cancer. *Life Sci* 2020;251:117604.
35 Bezu L, Wu Chuang A, Humeau J, *et al*. Quantification of eIF2alpha phosphorylation during immunogenic cell death. *Methods Enzymol* 2019;629:53–69.
36 Cerrato G, Humeau J, Sauvat A, *et al*. Assessment of transcription inhibition as a characteristic of immunogenic cell death. *Methods Cell Biol* 2022. doi:10.1016/bs.mcb.2021.12.026
37 Sauvat A, Cerrato G, Humeau J, *et al*. High-Throughput label-free detection of DNA-to-RNA transcription inhibition using brightfield microscopy and deep neural networks. *Comput Biol Med* 2021;133:104371.
38 Cerrato G, Liu P, Martins I, *et al*. Quantitative determination of phagocytosis by bone marrow-derived dendritic cells via imaging flow cytometry. *Methods Enzymol* 2020;632:27–37.
39 Enot DP, Vacchelli E, Jacquelot N, *et al*. TumGrowth: an open-access web tool for the statistical analysis of tumor growth curves. *Oncoimmunology* 2018;7:e1462431.
40 Lévesque S, Le Naour J, Pietrocola F, *et al*. A synergistic triad of chemotherapy, immune checkpoint inhibitors, and caloric restriction mimetics eradicates tumors in mice. *Oncoimmunology* 2019;8:e1657375.
41 Benayahu D, Shur I, Marom R, *et al*. Cellular and molecular properties associated with osteosarcoma cells. *J Cell Biochem* 2001;84:108–14.
42 Martins I, Kepp O, Schlemmer F, *et al*. Restoration of the immunogenicity of cisplatin-induced cancer cell death by endoplasmic reticulum stress. *Oncogene* 2011;30:1147–58.
43 Senovilla L, Vitale I, Martins I, *et al*. An immunosurveillance mechanism controls cancer cell ploidy. *Science* 2012;337:1678–84.
44 Klionsky DJ, Abdel-Aziz AK, Abdelfatah S, *et al*. Guidelines for the use and interpretation of assays for monitoring autophagy (4th edition)[1]. *Autophagy* 2021;17:1–382. Jan.
45 Nascimbeni AC, Codogno P, Morel E. Local detection of PtdIns3P at autophagosome biogenesis membrane platforms. *Autophagy* 2017;13:1602–12.
46 Kimura S, Noda T, Yoshimori T. Dissection of the autophagosome maturation process by a novel reporter protein, tandem fluorescent-tagged LC3. *Autophagy* 2007;3:452–60.
47 Tallóczy Z, Jiang W, Virgin HW, *et al*. Regulation of starvation- and virus-induced autophagy by the eIF2alpha kinase signaling pathway. *Proc Natl Acad Sci U S A* 2002;99:190–5.
48 Høyer-Hansen M, Jäättelä M. Connecting endoplasmic reticulum stress to autophagy by unfolded protein response and calcium. *Cell Death Differ* 2007;14:1576–82.
49 Kroemer G, Mariño G, Levine B. Autophagy and the integrated stress response. *Mol Cell* 2010;40:280–93.
50 Donnelly N, Gorman AM, Gupta S, *et al*. The eIF2α kinases: their structures and functions. *Cell Mol Life Sci* 2013;70:3493–511.
51 Harding HP, Zhang Y, Bertolotti A, *et al*. Perk is essential for translational regulation and cell survival during the unfolded protein response. *Mol Cell* 2000;5:897–904.
52 Wu Q, Tian A-L, Durand S, *et al*. Isobacachalcone induces autophagy and improves the outcome of immunogenic chemotherapy. *Cell Death Dis* 2020;11:1015.
53 Pozzi C, Cuomo A, Spadoni I, *et al*. The EGFR-specific antibody cetuximab combined with chemotherapy triggers immunogenic cell death. *Nat Med* 2016;22:624–31.
54 Kroemer G, Galassi C, Zitvogel L, *et al*. Immunogenic cell stress and death. *Nat Immunol* 2022. doi:10.1038/s41590-022-01132-2. [Epub ahead of print: 10 Feb 2022].
55 Tsuchiya H, Mizogami M, Ueno T, *et al*. Cardiotoxic local anesthetics increasingly interact with biomimetic membranes under ischemia-like acidic conditions. *Biol Pharm Bull* 2012;35:988–92.
56 Grishko V, Xu M, Wilson G, *et al*. Apoptosis and mitochondrial dysfunction in human chondrocytes following exposure to lidocaine, bupivacaine, and ropivacaine. *J Bone Joint Surg Am* 2010;92:609–18.
57 Weinberg GL, Palmer JW, VadeBoncouer TR, *et al*. Bupivacaine inhibits acylcarnitine exchange in cardiac mitochondria. *Anesthesiology* 2000;92:523–8.
58 Onizuka S, Yonaha T, Tamura R, *et al*. Lidocaine depolarizes the mitochondrial membrane potential by intracellular alkalization in rat dorsal root ganglion neurons. *J Anesth* 2011;25:229–39.
59 Onizuka S, Tamura R, Yonaha T, *et al*. Clinical dose of lidocaine destroys the cell membrane and induces both necrosis and apoptosis in an identified Lymnaea neuron. *J Anesth* 2012;26:54–61.
60 Perez-Castro R, Patel S, Garavito-Aguilar ZV, *et al*. Cytotoxicity of local anesthetics in human neuronal cells. *Anesth Analg* 2009;108:997–1007.
61 Johnson ME, Uhl CB, Spittler K-H, *et al*. Mitochondrial injury and caspase activation by the local anesthetic lidocaine. *Anesthesiology* 2004;101:1184–94.
62 Gottfried E, Kreutz M, Mackensen A. Tumor metabolism as modulator of immune response and tumor progression. *Semin Cancer Biol* 2012;22:335–41.
63 Cata JP, Ramirez MF, Velasquez JF, *et al*. Lidocaine stimulates the function of natural killer cells in different experimental settings. *Anticancer Res* 2017;37:4727–32.
64 Schlagenhauff B, Ellwanger U, Breuninger H, *et al*. Prognostic impact of the type of anaesthesia used during the excision of primary cutaneous melanoma. *Melanoma Res* 2000;10:165–9.
65 Biki B, Mascha E, Moriarty DC, *et al*. Anesthetic technique for radical prostatectomy surgery affects cancer recurrence: a retrospective analysis. *Anesthesiology* 2008;109:180–7.
66 Exadaktylos AK, Buggy DJ, Moriarty DC, *et al*. Can anesthetic technique for primary breast cancer surgery affect recurrence or metastasis? *Anesthesiology* 2006;105:660–4.
67 Christopherson R, James KE, Tableman M, *et al*. Long-term survival after colon cancer surgery: a variation associated with choice of anesthesia. *Anesth Analg* 2008;107:325–32.
68 de Oliveira GS, Ahmad S, Schink JC, *et al*. Intraoperative neuraxial anesthesia but not postoperative neuraxial analgesia is associated with increased relapse-free survival in ovarian cancer patients after primary cytoreductive surgery. *Reg Anesth Pain Med* 2011;36)::271–7. May-Jun;.
69 Gupta A, Björnsson A, Fredriksson M, *et al*. Reduction in mortality after epidural anaesthesia and analgesia in patients undergoing rectal but not colonic cancer surgery: a retrospective analysis of data from 655 patients in central Sweden. *Br J Anaesth* 2011;107:164–70.
70 Lin L, Liu C, Tan H, *et al*. Anaesthetic technique may affect prognosis for ovarian serous adenocarcinoma: a retrospective analysis. *Br J Anaesth* 2011;106:814–22.
71 Weng M, Chen W, Hou W, *et al*. The effect of neuraxial anesthesia on cancer recurrence and survival after cancer surgery: an updated meta-analysis. *Oncotarget* 2016;7:15262–73.
72 Ramirez MF, Tran P, Cata JP. The effect of clinically therapeutic plasma concentrations of lidocaine on natural killer cell cytotoxicity. *Reg Anesth Pain Med* 2015;40:43–8.
73 Wu Chuang A, Kepp O, Kroemer G, *et al*. Direct cytotoxic and indirect, immune-mediated effects of local anesthetics against cancer. *Front Oncol* 2021;11:821785.